

Benchmarking Recursive-Collapse Warning Claims Under Matched False-Positive Control

David Mullett

Independent Researcher

ORCID: 0009-0004-2543-1664

Corresponding author: David Mullett · d@loopzero.org

One-Sentence Summary

A matched-FP benchmark for recursive collapse: signature directionally aligned across domains; no detector accepted.

Abstract

Recursive systems can enter collapse-like regimes — self-reinforcing amplification, persistent recursion, and narrowing diversity that mask accelerating internal degradation — before overt failure becomes visible. We introduce Loopzero, a claim-bounded benchmark framework for testing whether recursive failures follow a directional telemetry pattern: rising gain (G), recursive persistence (p), and declining diversity (δ). The claim boundary is specified in Lean; the Lean artifact does not verify real telemetry, benchmark validity, or detector performance.

We evaluate the bridge on two frozen public-artifact benchmarks: a segmented public-markets benchmark (Volmageddon 2018, COVID MWCB 2020) and a MovieLens-25M offline deterministic recommender replay. Detectors are evaluated under a locked equal-false-positive contract ($FP \in [0.03, 0.07]$, pre-registered) so all configurations face the same alert budget. Neither tested standard comparators nor Loopzero’s pre-registered quantile detector achieved an accepted operating point. Directional witness alignment held on both canonical benchmarks, with adjacent-horizon and row-level limitations disclosed. Digitized Shumailov et al. (2024) LLM training-loop trajectories are directionally consistent with the pattern; matched-FP evaluation in that domain is deferred.

The contribution is a reproducible, falsifiable benchmark framework for evaluating recursive-collapse warning claims under an explicit alert-budget contract — non-acceptance reported as a first-class scientific outcome.

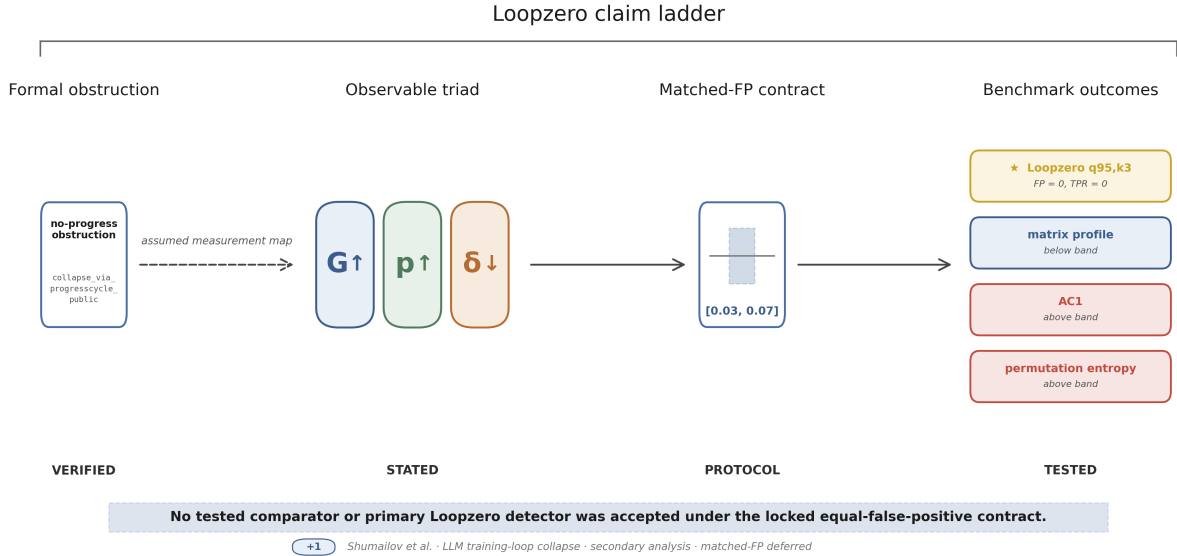


Figure 1. Loopzero claim ladder: from Lean-checked obstruction to empirical benchmark claims. Across the canonical public-markets and MovieLens-25M recommender benchmarks, no tested comparator configuration achieved acceptance under the locked equal-false-positive band $[0.03, 0.07]$: matrix profile (FP = 0.014, under-band) and AC1 (FP = 0.132, over-band) are illustrative cases shown; permutation entropy (FP = 0.368, far above band) completes the calibration outcome. The figure decomposes the underlying claim into four epistemic layers: (i) an elementary no-progress obstruction verified in Lean (`collapse_via_progresscycle_public`); (ii) an assumed measurement map to observable $G/p/\delta$ telemetry, stated as a conditional bridge; (iii) the matched-false-positive protocol; and (iv) empirical testing on frozen public-artifact benchmarks. Comparator markers are color-coded by failure mode (blue = under-band; orange = over-band). Sample sizes: canonical segmented markets $n_{\text{control}}=38 + n_{\text{event}}=16$; canonical recommender at $h=50$ $n_{\text{control}}=4,755 + n_{\text{event}}=35,584$ (40,339 user clusters total). The Shumailov et al. model-collapse analysis is included as a secondary directional-consistency check only; matched-FP evaluation in that domain is deferred.

Introduction

A formally specified obstruction for recursive collapse

Many systems of scientific and practical interest are recursive: present state shapes future state, and locally valid updates can reinforce their own continuation. Collapse, catastrophic shift, and resilience loss are well-established phenomena in complex systems (Scheffer et al., 2001; Holling, 1973). In such recursive systems, collapse need not begin as overt breakdown. Related recursive-collapse behavior has recently been demonstrated in generative-model training loops, where repeated training on recursively generated data degrades model behavior (Shumailov et al., 2024). Building on the established early-warning and critical slowing down literature, which has developed variance growth, autocorrelation shifts, and threshold excursions as observables for critical-transition detection (Scheffer et al., 2009; Scheffer et al., 2012; Carpenter et al., 2011; Dakos et al., 2012), this paper begins from a complementary starting point: a formally specified structural obstruction characterizing one specific failure mode within the broader recursive-collapse landscape. The empirical evaluation focuses on digital recursive systems — segmented public-markets telemetry and an offline deterministic recommender — with the

Shumailov training-loop setting included as a secondary consistency check; the formal obstruction itself is intended to apply more broadly.

We formalize this as a no-progress obstruction for recursive feedback systems, verified in Lean (de Moura & Ullrich, 2021; The mathlib Community, 2020). In that formal setting, one strictly worsening update coupled to monotone tethers can generate a cycle in which local continuation remains possible while meaningful progress is lost. In plain terms, a no-progress obstruction is a condition under which a system keeps taking valid local steps yet never actually improves. A monotone tether is a quantity constrained to move in one direction only — able to hold or worsen, but not recover. The empirical question is therefore not whether one can engineer a useful detector from arbitrary signals. It is whether this no-progress obstruction admits a conditional bridge, under stated assumptions, to a measurable pre-collapse footprint in observed recursive systems.

The formal obstruction is intentionally elementary; the Lean development is not presented as a substantive contribution in formal methods. Its purpose is to specify the claim boundary in machine-checkable form, so that the formal/empirical divide is explicit and inspectable. The Lean artifact contains three components: an abstract no-progress obstruction over preorders, a measurement-map bridge, and a schematic G, p, δ -style telemetry specialization. A preorder here is simply a ranking of system states by ‘at least as good as’ that allows ties and pairs that need not be directly comparable. The measurement map is the assumed link from observable telemetry to that ranking, which the paper assumes rather than proves. Lean verifies the structural ordered-measurement obstruction and the schematic telemetry specialization; it does not verify that real benchmark telemetry supplies the required measurement map. The empirical claims in this paper depend on the bridge protocol described below, not on the formal artifact.

Conditional telemetry bridge

The formal result does not itself specify a unique empirical measurement scheme for collapse. Cascading failure in interdependent systems provides structural motivation for treating recursive no-progress as a distinct failure mode (Buldyrev et al., 2010). The formal result identifies a class of recursive no-progress regimes in which local continuation remains possible while meaningful forward improvement becomes inaccessible. We therefore treat the bridge as conditional rather than automatic: to relate the obstruction to data, we consider recursive systems in which future updates depend partly on recent internal outputs, partly on external input, and partly on the diversity of accessible next states. Under this interpretation, collapse need not first appear as abrupt breakdown. It may instead emerge as an observable pre-collapse regime in which perturbations are increasingly amplified, recent internally generated states increasingly determine subsequent states, and the accessible state space contracts.

The empirical claim that real benchmark telemetry supplies such a measurement map remains external to Lean. It is tested by the benchmark protocol: the observed G, p, δ witnesses must satisfy the prespecified bridge criterion before externally defined collapse events under the locked false-positive contract, while comparator families are evaluated under the same alert budget.

The obstruction therefore motivates three testable observable tendencies before externally defined collapse events. First, rising gain G , indicating amplification rather than damping of perturbation. Second, rising recursive persistence p (operationalized in the bridge criterion as a non-relaxation gate), indicating increasing persistence of internally generated state. Third, declining diversity δ , indicating contraction of the effective range of system trajectories (Walker et al., 2004; Gao et al., 2016). We use G , p , and δ as empirical proxies for amplification, recursive persistence,

and state-space contraction. This bridge is explicitly falsifiable. It would be weakened if benchmark-defined collapse repeatedly occurred without prior elevation of G and p and reduction of δ , or if matched-false-positive comparator configurations repeatedly recovered accepted operating points without this triad.

Scope summary. (i) Lean verifies the abstract no-progress obstruction over preorders, the bridge lemma `collapse_via_progresscycle_public`, and a schematic telemetry specialization. (ii) The conditional bridge assumes that real recursive systems admit a measurement function μ mapping observable telemetry into a preorder, under which the witness triad’s directional structure (rising G , rising p , declining δ) corresponds to the formal no-progress condition. (iii) The benchmarks test whether the witness pattern in fact precedes externally defined event labels under the locked equal-false-positive contract; this is an empirical question, not a verified one.

Telemetry witnesses and matched-false-positive benchmarking

The bridge criterion is operationalized through a triplet of witnesses. G estimates short-horizon amplification of perturbation, p estimates short-horizon recursive persistence of active state, and δ estimates the effective breadth of observed system behavior across channels, modes, or trajectories. The predicate is therefore designed to test the empirical signature implied by the formal mechanism, not to restate the formal obstruction in observational language.

In the current implementation, the three witnesses are not equally directional in their operational role. G is evaluated as an elevated-gain condition relative to recent background, and δ is evaluated through a non-increase condition over the relevant lookback window. The p witness is used most conservatively: it functions as a non-relaxation gate consistent with monotone-tether semantics rather than as a standalone directional effect-size claim. In the public-markets adapter, p is constructed from a trailing recurrence statistic over stress events defined using a fixed z -threshold of 1.5; this threshold is part of the current adapter definition and should be interpreted as such.

All empirical evaluation is conducted under a matched false-positive contract. In heterogeneous systems, comparator families can appear competitive simply by spending false alarms differently (Boettiger & Hastings, 2012a; Jäger & Füllsack, 2019). We therefore compare detectors only at the same alert budget, defined by a locked equal-false-positive criterion rather than by arbitrary family-specific thresholds (Boettiger & Hastings, 2012b; Hanley & McNeil, 1982). A configuration is accepted only if its control-unit false-positive rate lies within the prespecified interval $FP \in [0.03, 0.07]$.

The acceptance band was chosen prior to evaluation to reflect the operational alert burden plausible for an operator monitoring a comparator unit population over a comparable observation period. A mean false-positive rate of 0.05 corresponds to approximately one false alert per 20 control-period units; the half-width of ± 0.02 reflects acceptable sampling variation under finite-control evaluation. Tighter bands such as $[0.01, 0.05]$ would be operationally desirable but require larger control-unit populations than the canonical markets benchmark provides; wider bands such as $[0.05, 0.10]$ would inflate the false-alarm budget beyond what is operationally tolerable in a deployed warning context. The band was locked at this specification before any comparator evaluation. We note that on the canonical markets benchmark with $n=38$ controls, the grid step $1/38 = 0.026316$ admits only 2/38 control alarms within the band ($FP = 0.052632$), making the band effectively a single-grid-point target on that benchmark; the recommender benchmark with $n=4,755$ controls (grid step $1/4755 = 0.0002103$) is therefore the empirically dispositive case, and the markets non-acceptance result should be read as corroborating second-domain evidence rather than as an independent statistical

claim of comparator inadequacy.

Under this contract, the comparator-non-recovery claim is directly falsifiable: it fails if any comparator configuration admits an accepted operating point on the canonical benchmark under the same criterion. An operating point is one setting at which a detector runs, fixing its false-positive and true-positive rates. It counts as accepted only if its false-positive rate falls inside the locked band [0.03, 0.07].

Results

Cross-domain evidence for a pre-collapse signature

We therefore test whether the witness triad (G , p , δ) appears before externally defined collapse events under a locked equal-false-positive benchmark across heterogeneous recursive systems. Across retained domain families, the witness triad aligns directionally ahead of externally defined breakdown or intervention points and does so under the same alert-budget rule. These retained families were chosen not because they are easy cases, but because they admit externally defined event times, nontrivial controls, and fair comparator evaluation under a common false-positive contract.

Directional witness summaries were fully aligned on the canonical recommender benchmark. On the canonical public-markets benchmark, the same directional pattern was recovered when markets were summarized over the last 30 minutes of each exact canonical unit using G , p , and diversity-change within the late window. In a wider 60-minute markets summary, G and p remained directionally aligned whereas diversity-change weakened. We therefore interpret the markets bridge as localized and late-window strongest rather than uniformly invariant across wider summary windows.

Per-witness effect-size summaries extend this directional analysis to magnitude and uncertainty. We compute Cohen’s d , Glass’s d , and rank AUC for each witness (G , p , δ) at each benchmark/horizon, with cluster-aware bootstrap 95% BCa confidence intervals over 10,000 iterations (markets: segment-level resampling, $n=38$ controls + 16 events; recommender: user-level resampling, $n = 40,339$ user clusters). At the canonical recommender horizon $h=50$, all three witnesses point in the predicted direction with intervals clear of the null reference (G Cohen’s $d = +0.10$ [+0.08, +0.12]; p Cohen’s $d = +0.08$ [+0.05, +0.11]; δ Cohen’s $d = -0.17$ [-0.21, -0.13]). At adjacent horizons the pattern degrades asymmetrically: at $h=40$ the G witness flips to a wrong-direction effect ($d = -0.21$) while p and δ hold in the predicted direction; at $h=60$ G strengthens further ($d = +0.33$) while p and δ collapse to null intervals. The pre-registered canonical horizon is therefore the only configuration where all three witnesses align in the predicted direction with intervals clear of null. On the markets benchmark, per-row effect sizes are uniformly null across all three witnesses (intervals span the null reference); the markets directional pattern reported above is recovered at the unit-level aggregation grain used in the late-window analysis (mean per segment, then compare across $n=38+16$ segments), not at the per-row grain on which these effect sizes are computed. A full effect-size table with both BCa and percentile CIs is reported in Supplementary Table S2; Figure 6 provides a forest-plot visualization.

The broader significance is not that a new warning statistic works in one domain. It is that a no-progress obstruction appears to support a domain-resolved empirical signature across systems that differ strongly in substrate, timescale, and external semantics. The evidence therefore supports an explicitly bounded empirical program rather than a single-domain detector construction.

A domain-resolved witness-direction summary is provided in the Supplementary Materials. The

combined comparator calibration summary across both flagship benchmarks is reported in Table 1.

Table 1. Matched false-positive evaluation on frozen public-artifact benchmarks under the locked equal-false-positive contract ($FP \in [0.03, 0.07]$). Panels: markets (n=38 controls + 16 events on `voldageddon_covid_public_v2`) and canonical recommender (n=4,755 controls + 35,584 events at horizon $h=50$ on `movielens25m_recursive_frontier_public_v1`; 40,339 user clusters total). Standard comparator families and Loopzero’s pre-registered quantile detector were evaluated under the same locked equal-false-positive contract. No tested comparator configuration and no operating point of Loopzero’s pre-registered quantile detector achieved an accepted operating point on either benchmark. The directional $G/p/\delta$ bridge summaries are therefore reported separately from binary detector acceptance.

Loopzero’s pre-registered quantile detector ($G > 95$ th percentile, $p > 95$ th percentile, $\delta < 5$ th percentile of control-unit reference rows; $k = 3$ consecutive windows) is evaluated at its pre-registered primary operating point on both canonical benchmarks. On the canonical markets benchmark (1,120 reference rows from 38 control units), the detector alarms 0 of 38 control units ($FP = 0.000$) and 0 of 16 event units (event alarm rate = 0.000). On the canonical recommender benchmark (47,550 reference rows from 4,755 control units), the detector alarms 0 of 4,755 control units ($FP = 0.000$) and 0 of 35,584 event units (event alarm rate = 0.000). The pre-registered operating point therefore falls under-band on both benchmarks. No tested operating point in either benchmark’s locked equal-FP band $[0.03, 0.07]$ achieves event recovery; full 9-cell $q \times k$ sensitivity grids per benchmark are reported in `results/rendered/bridge/a1_loopzero_operating_point_s.md`, and the pre-registered specification is documented in `analysis/14_a1_prereg.md`. Under matched-FP discipline, Loopzero’s pre-registered detector and the tested standard comparator families therefore both report non-acceptance on the canonical benchmarks. This consistency is itself a coherent outcome of the matched-FP framework, which evaluates detectors on a level playing field rather than at family-specific thresholds; the manuscript’s central comparator-non-recovery claim and the bridge-criterion directional analysis (witnesses G , p , δ separating event from control rows in the prespecified directions on the canonical recommender benchmark and on the canonical late-window markets summary) are unaffected by this detector-specific non-acceptance result.

Benchmark	Comparator (family, role)	Configuration	Control FP	Event alarm rate	Distance from band	Status
Markets (n=38 controls, 16 events)	AC1 (fast — nearest nontrivial)	<code>ac1_ews_</code> <code>_632f23b</code> 2	0.1316 (5/38)	0.0625 (1/16)	+0.0616 above	Above band
Markets	Permutation entropy (slow — best nontrivial)	<code>permutat</code> <code>ion_entr</code> <code>opy__259</code> <code>c1b96</code>	0.3684 (14/38)	0.2500 (4/16)	+0.2984 above	Above band

Benchmark	Comparator (family, role)	Configuration	Control FP	Event alarm rate	Distance from band	Status
Markets	Matrix profile / permutation entropy (slow — numerically nearest)	trivial-silent ties	0.0000 (0/38)	0.0000 (0/16)	—	Trivial-silent
Recommender (n=4,755 controls, 35,584 events; 105 configurations tested)	Matrix profile (slow — overall nearest)	<code>matrix_p</code> <code>rofile__</code> <code>44b81bd6</code>	0.01367	0.1107	−0.0163 below	Below band
Recommender	Variance EWS (fast — nearest)	trivial-silent	0.0000	—	—	Trivial-silent

No tested comparator configuration achieved an accepted operating point on either benchmark. Comparator calibration under the matched false-positive contract is not equivalent to universal detector ranking; comparators and Loopzero’s pre-registered detector may admit competitive operating points under different evaluation frameworks. The contract evaluates whether the prespecified canonical band can be reached, not which detector is universally superior.

Canonical public recommender benchmark

A second flagship benchmark was constructed from MovieLens-25M user trajectories to test whether the bridge criterion survives outside markets. Recommender systems are known to narrow accessible diversity through feedback-driven filtering (Fleder & Hosanagar, 2009). User ratings were sorted chronologically, reduced to one episode per user, and replayed under a deterministic item-item collaborative-filtering engine with a warm-start prefix and a held-out positive frontier (Chaney et al., 2018; Jiang et al., 2019; Mansoury et al., 2020). On the canonical 50-step benchmark, 40,339 user-level units satisfied inclusion criteria, including 35,584 event units and 4,755 control units. The control-unit false-positive grid step was $1/4755 = 0.0002103$, so the prespecified acceptance band $[0.03, 0.07]$ was reachable by construction.

On this canonical recommender benchmark, the witness pattern satisfied the prespecified bridge criterion in the pre-collapse window: pre-collapse event units showed higher amplification G , higher recursive persistence p , and lower diversity δ than reference controls. User-level bootstrap summaries were directionally consistent with this pattern and were used descriptively rather than as a significance test. Under the same locked equal-false-positive contract, no tested fast or slow comparator configuration admitted an accepted operating point. Across 105 tested configurations, the overall nearest comparator was matrix profile (`matrix_profile__44b81bd6`), which remained

below the lower edge of the accepted band with control FP = 0.0136698, band distance = 0.0163302, and event alarm rate = 0.110668. Among fast families, the numerically nearest operating point was a trivial-silent variance EWS configuration at FP = 0.0, whereas the nearest nontrivial fast-family configurations overfired controls substantially.

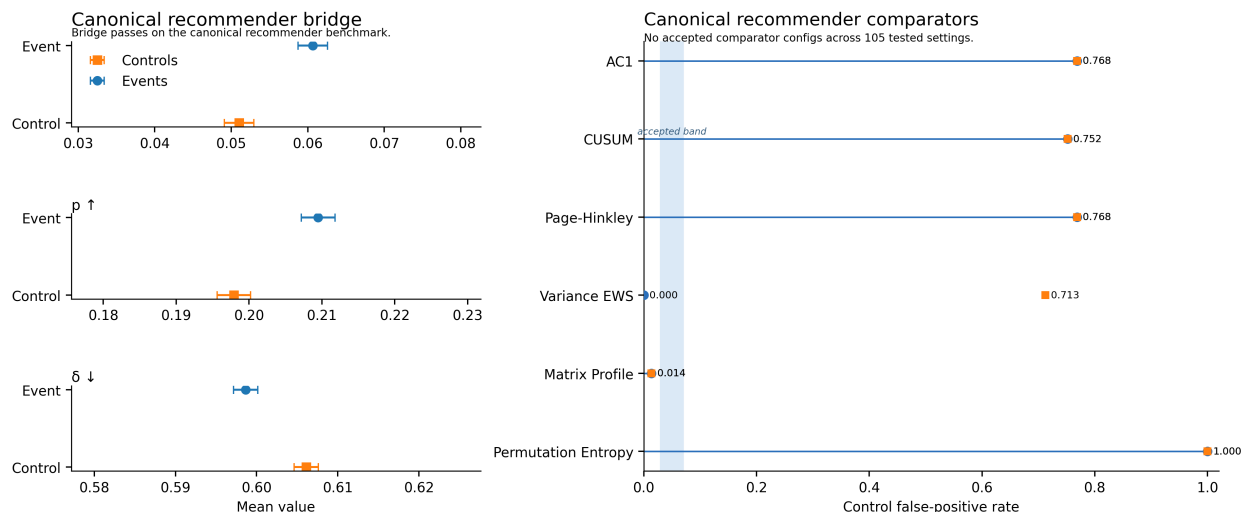


Figure 2. Canonical recommender benchmark: bridge summary and comparator calibration. On the canonical 50-step MovieLens-25M recursive frontier benchmark ($n=4,755$ control units + 35,584 event units = 40,339 user clusters total at horizon $h=50$), directional witness summaries are fully aligned: event units show higher gain G , higher recursive persistence p , and lower diversity δ than controls. Under the same locked equal-false-positive contract, no tested comparator configuration is accepted across 105 tested settings; the overall nearest comparator is matrix profile at FP = 0.014, below the lower edge of the accepted band. Directional witness alignment in this canonical $h=50$ panel is small in magnitude ($G \text{ d} \approx +0.10$, $p \text{ d} \approx +0.08$, $\delta \text{ d} \approx -0.17$); the bridge claim is a directional one and is not equivalent to a claim of large discriminative effect size. Effect-size estimates and BCa intervals are reported in Figure 6 and Supplementary Table S2. Results are based on offline deterministic replay rather than deployed-system feedback.

Recommender robustness under adjacent horizon sensitivity

To test whether the recommender result depended on the canonical episode horizon, the benchmark was rebuilt at adjacent horizons of 40 and 60 recursive update steps while holding benchmark construction and comparator rules fixed. At both adjacent horizons, no comparator configuration recovered an accepted operating point under the locked equal-false-positive band. The overall nearest comparator remained matrix profile in all three horizon settings and remained outside the accepted interval. The bridge degrades asymmetrically across adjacent horizons. At $h=40$, witnesses p and δ remain aligned in the predicted direction with bootstrap CIs clear of null, but G 's sign reverses (events show lower gain than controls, opposite to the prediction). At $h=60$, G 's alignment strengthens, but bootstrap CIs for p and δ collapse to include null. The pre-registered canonical horizon $h=50$ is therefore the only tested configuration where all three witnesses simultaneously align in the predicted direction with bootstrap CIs clear of null (Supplementary Table S2). This asymmetric horizon dependence is consistent with witness-specific timescales — G is sensitive to cumulative amplification (favoring longer horizons) while p and δ measure within-trajectory recursive structure that becomes harder to distinguish from control trajectories

at longer horizons — and reinforces the load-bearing role of pre-registration for the bridge claim. Loopzero’s pre-registered quantile detector was also evaluated at its primary operating point ($q=95, k=3$) on both adjacent-horizon packets. On the recommender benchmark rebuilt at $h=40$ (65,620 reference rows from 6,562 control units), the detector alarms 0 of 6,562 control units (FP = 0.000) and 0 of 33,777 event units (event alarm rate = 0.000). On the recommender benchmark rebuilt at $h=60$ (39,960 reference rows from 3,996 control units), the detector alarms 0 of 3,996 control units (FP = 0.000) and 0 of 36,343 event units (event alarm rate = 0.000). The detector’s primary-cell non-acceptance pattern observed at $h=50$ therefore extends across all three tested horizons; full 9-cell $q \times k$ sensitivity grids at $h=40$ and $h=60$ are reported in `results/rendered/bridge/a1_loopzero_operating_points_h40_h60.md`. The recommender branch therefore supports a corroborating second flagship benchmark on the comparator claim, with a bounded robustness qualification on the bridge layer under adjacent horizon shortening rather than an unqualified invariance claim.

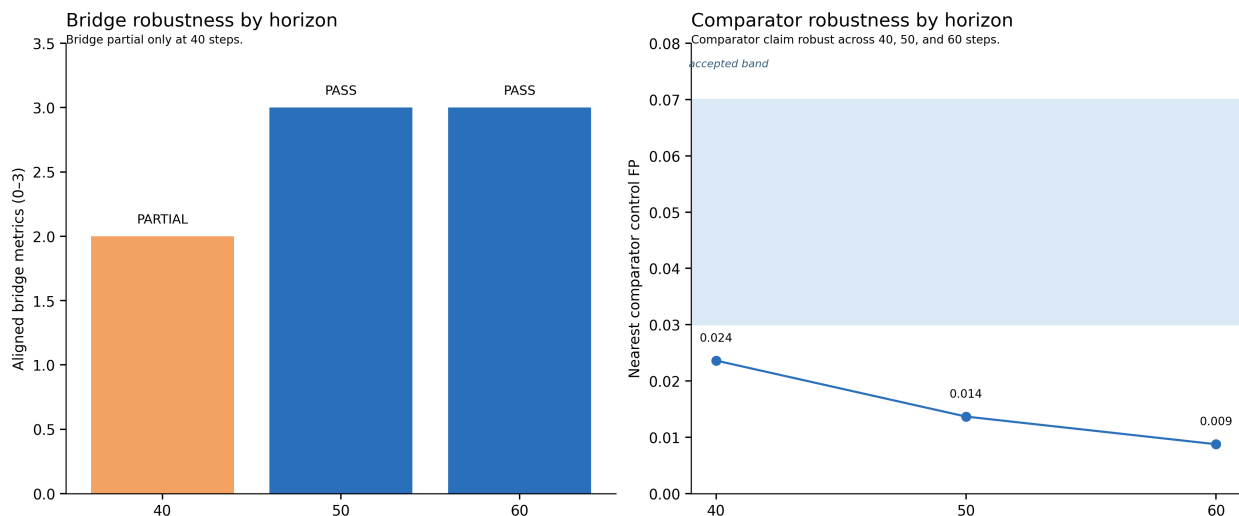


Figure 3. Recommender robustness by adjacent horizon sensitivity. Evaluation on the MovieLens-25M recursive frontier benchmark at three horizons (40,339 user clusters per panel; event/control splits vary by horizon — $h=40$: 33,777 events + 6,562 controls; $h=50$ canonical: 35,584 events + 4,755 controls; $h=60$: 36,343 events + 3,996 controls). The bridge criterion is satisfied at 50 and 60 steps and only partially satisfied at 40 steps, indicating bounded horizon sensitivity rather than failure of the empirical program. The comparator claim is robust across all three horizons: no tested comparator configuration is accepted at 40, 50, or 60 steps. PASS/PARTIAL refers exclusively to the prespecified direction-count bridge rule (event-unit G higher than control, p non-relaxation maintained, event-unit δ lower than control); it does not require effect-size intervals to exclude null. Per-horizon effect-size magnitudes and BCa intervals are reported in Figure 6 and Supplementary Table S2: $h=40$ shows G in the wrong direction ($d = -0.21$) with p and δ still aligned; $h=60$ shows G strengthening ($d = +0.33$) while p and δ effect-size intervals collapse to null. The pre-registered canonical horizon $h=50$ is the only configuration where all three witnesses align in the predicted direction with intervals clear of null. Results are based on offline deterministic replay rather than deployed-system feedback.

Public market event family

Public markets provide a stringent test because they combine exogenous shocks, endogenous amplification (Brunnermeier & Pedersen, 2009), volatility-linked stress indicators such as the VIX (Whaley, 2009; ESRB Advisory Scientific Committee, 2019), heterogeneous liquidity structure, and a substantial comparator literature. We therefore assembled a reproducible public market event family centered on the February 2018 Volmageddon dislocation (Augustin et al., 2021) and the March 2020 COVID market-wide circuit-breaker cluster (NYSE Market-Wide Circuit Breaker Working Group, 2021), together with hard negative controls. The purpose was not to present markets as a universal separator domain, but to ask whether a formally specified recursive warning criterion survives externally auditable benchmark construction in a domain with strong prior comparators and well-known confounds — macro-driven volatility, microstructure effects, calendar regularities, and news-shock dynamics that can produce volatility excursions without any underlying recursive feedback mechanism.

In this branch, the critical distinction is between narrative motivation and frozen benchmark evaluation. Narrative examples such as the 2010 Flash Crash (CFTC and SEC Staff, 2010) motivate the broader problem of recursive dislocation, but the quantitative claims reported here are anchored to the frozen canonical markets benchmark and its comparator contract. That benchmark is the relevant object for comparator availability, equal-false-positive reachability, and robustness.

Comparator calibration on the canonical markets benchmark

To test whether the markets result depended on a narrow comparator set, we evaluated a broader comparator suite on the canonical segmented markets benchmark, `volmageddon_covid_public_v2`, constructed from a single canonical source configuration and a rule in which one underlying market segment constituted one comparator unit. This yielded 38 control units and 16 event units, so the prespecified equal-false-positive acceptance band, $FP \in [0.03, 0.07]$, was reachable on this benchmark with grid step $1/38 = 0.026316$. Fast comparator families comprised variance EWS and lag-1 autocorrelation (AC1) (Dakos et al., 2012), CUSUM (Page, 1954), and Page-Hinkley (Page, 1954); slow families comprised matrix profile (Yeh et al., 2016) and permutation entropy (Bandt & Pompe, 2002). All families were evaluated under the same locked equal-false-positive contract with predeclared parameter grids, followed by full-grid expansion of the slow families on the frozen canonical benchmark. Two procedural filters apply during calibration: a `trivial_silent` flag identifies comparator configurations that emit zero alarms across the entire benchmark and therefore satisfy any false-positive band by vacuous compliance — these configurations are excluded from accepted-operating-point determination; an `unreachable_fp_band` filter excludes configurations whose minimum-length pre-conditions reduce `n_control_units` below the discrete-grid floor required to reach the $[0.03, 0.07]$ band, evaluated before calibration.

No tested fast or slow comparator configuration achieved the acceptance band on the canonical markets benchmark. The nearest nontrivial comparator remained AC1: configuration `ac1_ews__632f23b2` alarmed on 5/38 control units ($FP = 0.131579$) and 1/16 event units, leaving it 0.061579 above the admissible band. Full-grid slow-family evaluation did not rescue the comparator branch. The numerically nearest slow configurations were tied across matrix profile and permutation entropy, but both were trivial-silent, producing 0/38 control alarms and 0/16 event alarms. Among slow families, the best nontrivial configuration came from permutation entropy (`permutation_entropy__259c1b96`), which alarmed on 14/38 control units ($FP = 0.368421$) and 4/16 event units, remaining 0.298421 above band. Thus, under a reachable and

locked equal-false-positive criterion, no tested comparator configuration admitted an acceptable operating point on the canonical markets benchmark.

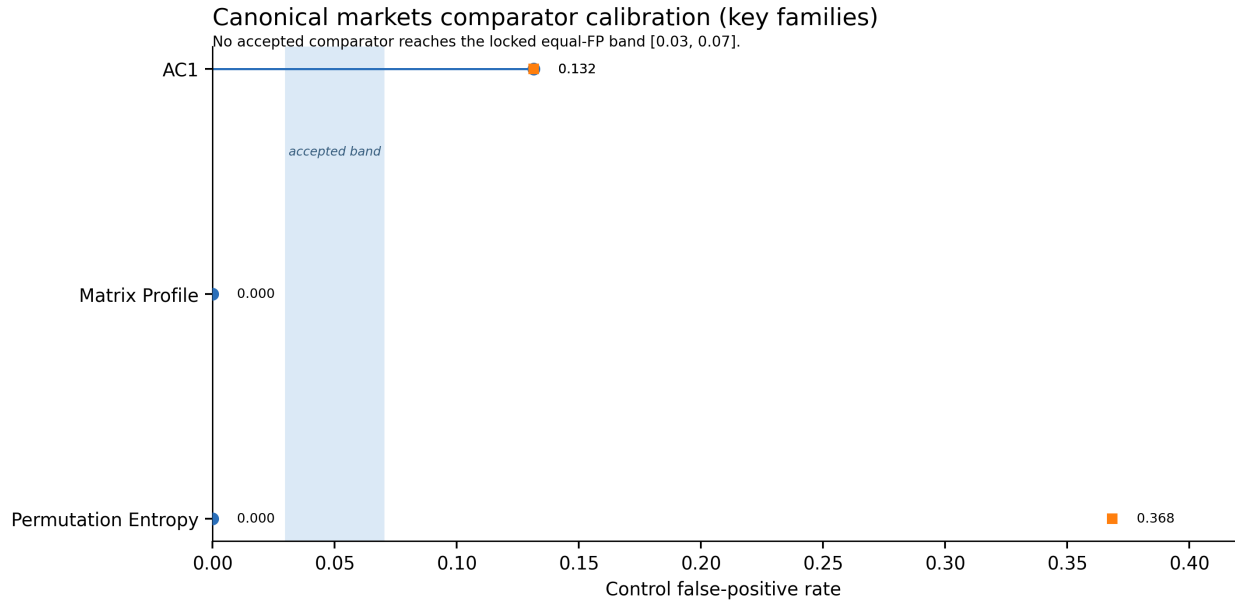


Figure 4. Comparator calibration on the canonical segmented markets benchmark (n=38 control units + 16 event units). No tested fast or slow comparator configuration reaches the locked equal-false-positive band [0.03, 0.07]. The nearest nontrivial comparator is AC1 at $FP = 0.131579$ (5/38 control alarm units), while the numerically nearest slow configurations are trivial-silent and the best nontrivial slow family, permutation entropy, remains materially above band.

Fast-family robustness under canonical and relaxed band specifications

The comparator conclusion in markets admits a narrower and more precise robustness statement. Under the prespecified equal-false-positive band [0.03, 0.07], no tested fast-family comparator configuration was accepted on the canonical 120-minute segmented markets benchmark or on 60-minute and 180-minute segmentation sensitivity variants. In all three cases, the nearest fast family remained AC1; the nearest false-positive rate was 0.1316 for the canonical 120-minute units, 0.0800 for the 60-minute units, and 0.1304 for the 180-minute units. Thus, fast-family non-acceptance was robust across tested segmentations at the locked canonical specification.

By contrast, post-processing band-sensitivity analysis showed that widening the acceptable interval to [0.02, 0.08] or [0.04, 0.08] admitted the 60-minute AC1 configuration, whereas the canonical 120-minute and 180-minute segmentations remained non-accepted. We therefore distinguish canonical robustness from relaxed-band sensitivity and do not claim full invariance to post hoc band relaxation. The result that carries manuscript weight is the stronger one: at the prespecified canonical band, no fast-family comparator is accepted at 60-, 120-, or 180-minute segmentation.

Controls, falsification boundary, and bounded exceptions

The bridge criterion is explicitly falsifiable. It would be weakened in four ways. First, if externally defined collapse events occurred without prior increase in G and p and decrease in δ . Second, if comparator configurations detected the same events under matched false-positive constraints

without exhibiting this triad. Third, if the (G, p, δ) pattern appeared frequently in control periods without progression toward externally defined collapse. Fourth, if alternative reasonable operationalizations of amplification, recursive persistence, and diversity contraction failed to agree directionally with the present measurements. At the benchmark level, the comparator non-recovery claim would fail if any tested comparator configuration achieved an accepted operating point on the canonical benchmark under the same equal-false-positive contract.

The markets branch also contains a bounded near-miss rather than a universal separator. Binary and topological diagnostics did not separate Volmageddon from vol-heavy hard negatives. The strongest remaining signal instead appeared in continuous witness quality, with the clearest confirmation in the corroborating intraday-grain witness configuration `cfg_002053`, particularly against the post-Volmageddon volatility-cluster control segment of February 8, 2018 (`volmageddon_control_2018_02_08`). We therefore treat this residual as a bounded exception that sharpens the empirical interpretation rather than as a contradiction of the broader result. Across the retained domains, neither the bridge criterion nor the comparator non-recovery claim is falsified.

Third-domain corroboration: LLM training-loop collapse (secondary analysis)

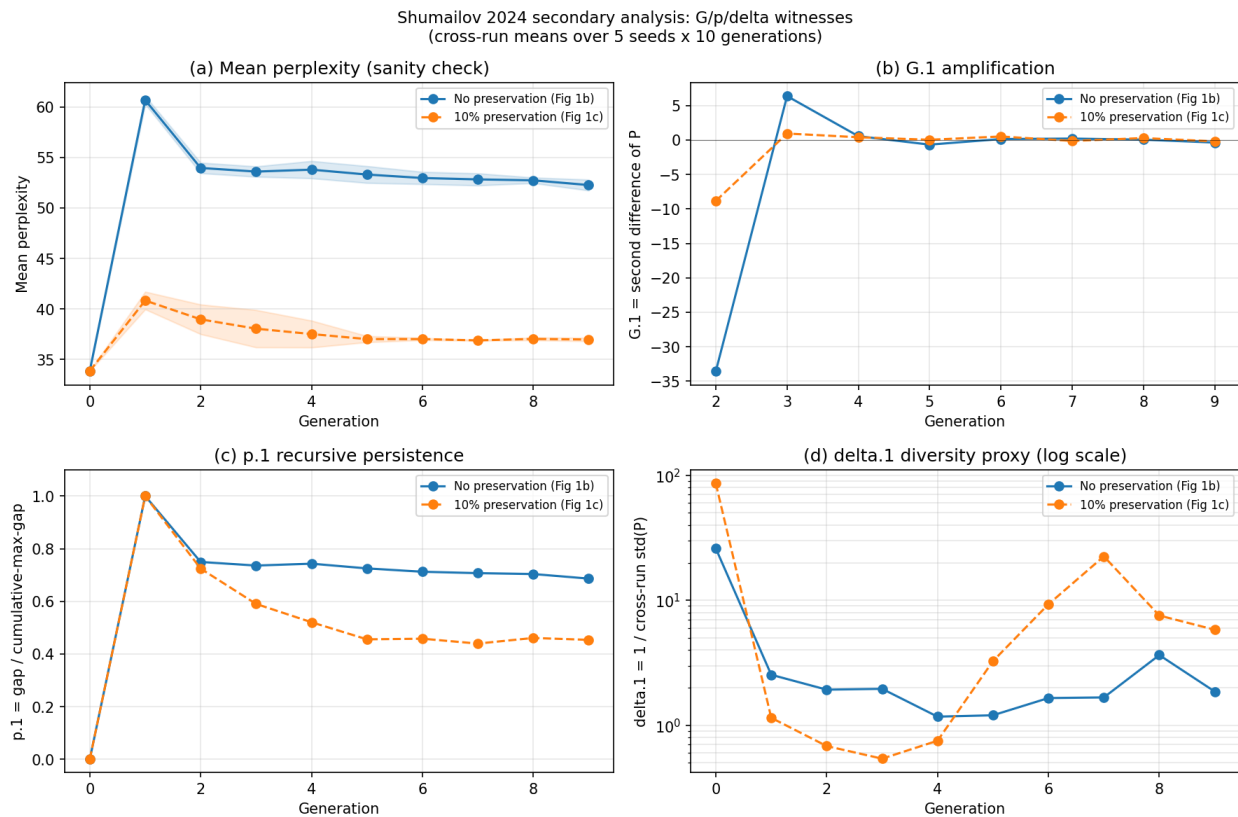


Figure 5. $G/p/\delta$ witnesses across 10 generations of recursive LLM fine-tuning, secondary analysis on data digitized from Shumailov et al. (2024) Figure 1b/1c right panels. Lines show cross-run means over 5 random-seed runs. (a) Mean perplexity sanity check with $\pm 1\sigma$ envelope. (b) G.1 amplification (second difference of mean perplexity per run); large negative deflection at generation 2 marks the phase-transition signature. (c) p.1 recursive persistence (gap-to-cumulative-max ratio); jumps to 1 at collapse onset and stays elevated. (d) $\delta.1$ diversity proxy (inverse cross-run perplexity standard deviation, log scale); declines sharply at onset in both regimes. Two regimes shown: no

preservation (blue, Fig 1b) and 10% real-data preservation (orange, Fig 1c).

Recursive language-model training exhibits the same closed-loop topology as the markets and recommender domains: model outputs become inputs to the next generation’s training, creating conditions for self-amplification and diversity contraction. Shumailov et al. (2024) demonstrated this empirically, showing that perplexity on held-out text rises sharply within one generation of fine-tuning on synthetic data and stabilizes at an elevated plateau, with magnitude depending on whether real data is preserved across generations. We use this third recursive domain as a directional-consistency check for the $G/p/\delta$ witness triad, conducted as secondary analysis rather than as a matched-FP benchmark.

We digitized mean perplexity values from Figure 1b/1c right panels of Shumailov et al. (five random-seed runs across ten recursive generations, in two preservation regimes: no preservation and 10% preservation). Each witness was computed from per-generation perplexity data: $G.1$ as the second difference of mean perplexity per run, $p.1$ as the ratio of the current perplexity-gap to the per-run cumulative-maximum gap, and $\delta.1$ as the inverse of cross-run perplexity standard deviation at each generation. Generation 0 (the Real wikitext2 baseline) is the control window; generations 1 through 9 are the event window. The Shumailov $G.1$ operationalization captures phase-transition magnitude ($|G|$ at onset) rather than the signed-elevation form used in the markets and recommender domains, reflecting that perplexity deviations in either direction can signal a regime shift in this setting.

All three witnesses move in the predicted direction across the collapse transition in both regimes (Figure 5). $G.1$ shows a sharp phase-transition signature: $|G|$ at generation 2 is $22.6\times$ the steady-state mean in the no-preservation regime and $16.7\times$ in the 10%-preservation regime. $p.1$ jumps from 0 at baseline to approximately 1 at generation 1 and never relaxes below 0.36 in either regime. $\delta.1$ declines sharply at onset (control/event ratio $13.3\times$ and $15.0\times$). The framework generates three graded predictions, all of which the data also support: $G.1$ transition magnitude scales with collapse severity ($3.8\times$ larger without preservation); $p.1$ plateau height encodes the regime (0.75 versus 0.45); $\delta.1$ partially recovers in the 10%-preservation regime as random seeds re-converge to a stable collapsed attractor.

We do not claim a third benchmark. Values are digitized from published figures rather than provided by the original authors, the $\delta.1$ operationalization captures inter-seed convergence rather than the within-model distributional diversity that the paper’s Theorem 3.1 directly addresses, and no comparator-acceptance evaluation under a matched false-positive contract was conducted for this domain. The full benchmark - including experimental pipeline reconstruction at scale and matched-FP evaluation - is deferred to follow-up work.

Cross-benchmark synthesis: effect sizes and comparator-band ROC

Figure 6 summarizes effect-size magnitudes and confidence intervals across all four benchmark/horizon configurations and all three witnesses. The visualization makes three findings inspectable at a glance. First, the canonical recommender horizon $h=50$ (blue, anchored by background tint) is the only configuration where all three witnesses align in the predicted direction with confidence intervals clear of the null reference. Second, adjacent recommender horizons degrade asymmetrically rather than uniformly: $h=40$ shows a wrong-direction effect on G with predicted-direction effects on p and δ , while $h=60$ shows a strong predicted-direction effect on G but null intervals on p and δ . Third, markets effects at the per-row grain are uniformly null across all three witnesses; the directional bridge claim for markets operates at the unit-level aggregation grain reported in the

late-window analysis. BCa and percentile confidence intervals agree to within Monte Carlo noise on all recommender cells ($n = 40,339$); they diverge meaningfully on markets cells, where the right-skewed bootstrap distribution at low n favors the BCa correction as the more honest read. Full effect-size numerics, including Glass's d and rank AUC alongside Cohen's d , are reported in Supplementary Table S2.

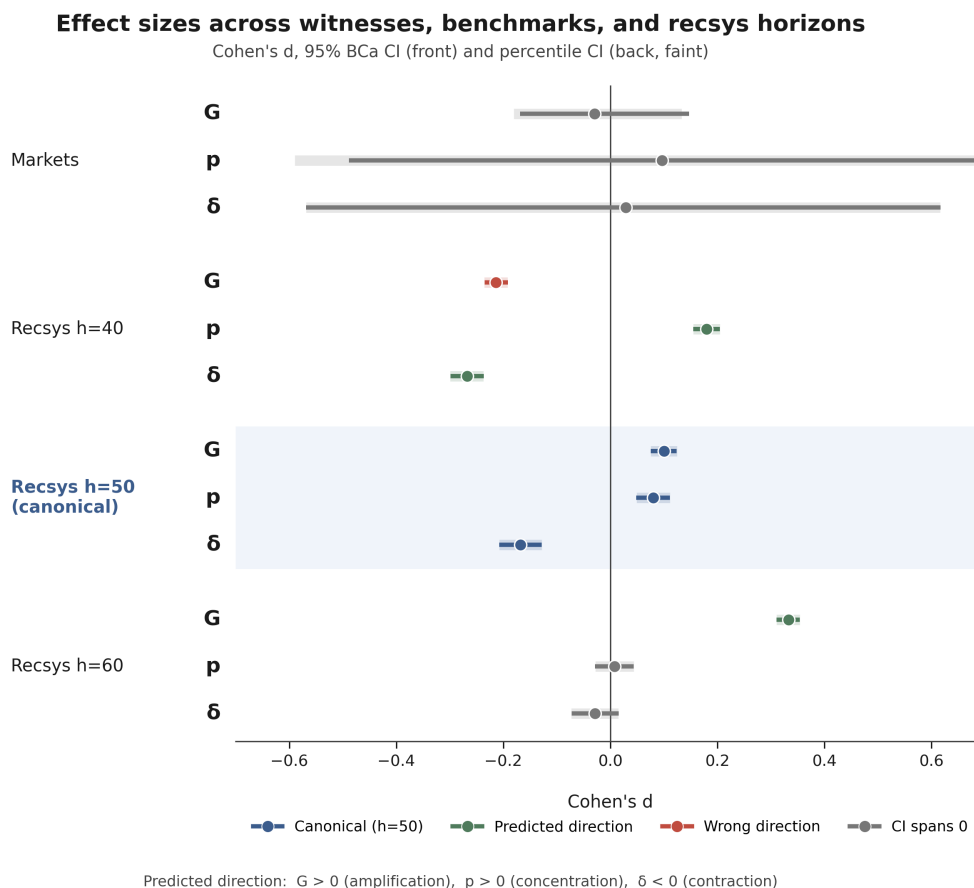


Figure 6. Effect sizes across witnesses, benchmarks, and recommender horizons. Cohen's d point estimates with 95% bias-corrected accelerated (BCa) confidence intervals in the foreground and 95% percentile confidence intervals in the faint background. Cluster-aware bootstrap (10,000 iterations) at segment-level grain for markets ($n=38$ controls + 16 events) and user-level grain for recommender ($n = 40,339$ user clusters per horizon panel; per-horizon event/control splits — $h=40$: $n_{\text{control}}=6,562$ / $n_{\text{event}}=33,777$; $h=50$ canonical: $n_{\text{control}}=4,755$ / $n_{\text{event}}=35,584$; $h=60$: $n_{\text{control}}=3,996$ / $n_{\text{event}}=36,343$; ~ 10 rows per cluster). Color coding: blue for the canonical $h=50$ group (anchored by background tint), green for predicted-direction effects with CIs clear of null, red for wrong-direction effects with CIs clear of null, gray for CIs spanning null. Predicted direction: $G > 0$ (amplification), $p > 0$ (concentration), $\delta < 0$ (contraction). The pre-registered canonical $h=50$ configuration is the only horizon where all three witnesses align in the predicted direction with intervals clear of null.

Figure 7 complements the effect-size synthesis with a direct visualization of how comparator families occupy the false-positive axis relative to the locked equal-FP band. Figure 6 quantifies how strongly witnesses separate event from control telemetry; Figure 7 quantifies how far each

comparator family operates from the contract-mandated acceptance region. Two findings sharpen the comparator-failure story. First, on the late-30-minute ROC slice the markets slow families (matrix profile, permutation entropy) fail at the data-availability gate before reaching calibration: this short window leaves $n_control_units = 6$, below the discrete-grid floor required to reach the $[0.03, 0.07]$ band, so they were filtered as `unreachable_fp_band` on this slice. These families are evaluated on the full-window canonical markets benchmark (Figure 4), where the nearest nontrivial slow configuration, permutation entropy, reaches 14/38 control units at $FP = 0.368$, above band. Second, the recommender slow families occupy the low-FP region but at very low TPR — visible in the inset zoom — making the FP/TPR trade-off inadequate for the contract at any horizon. The pre-registered Loopzero conservative operating point ($q=95, k=3$) is marked as a gold star at ($FP \approx 0, TPR \approx 0$); the achievable Loopzero envelope and its matched-FP comparison against the comparator suite are reported in the *Envelope-boundary matched-FP comparison* subsection below.

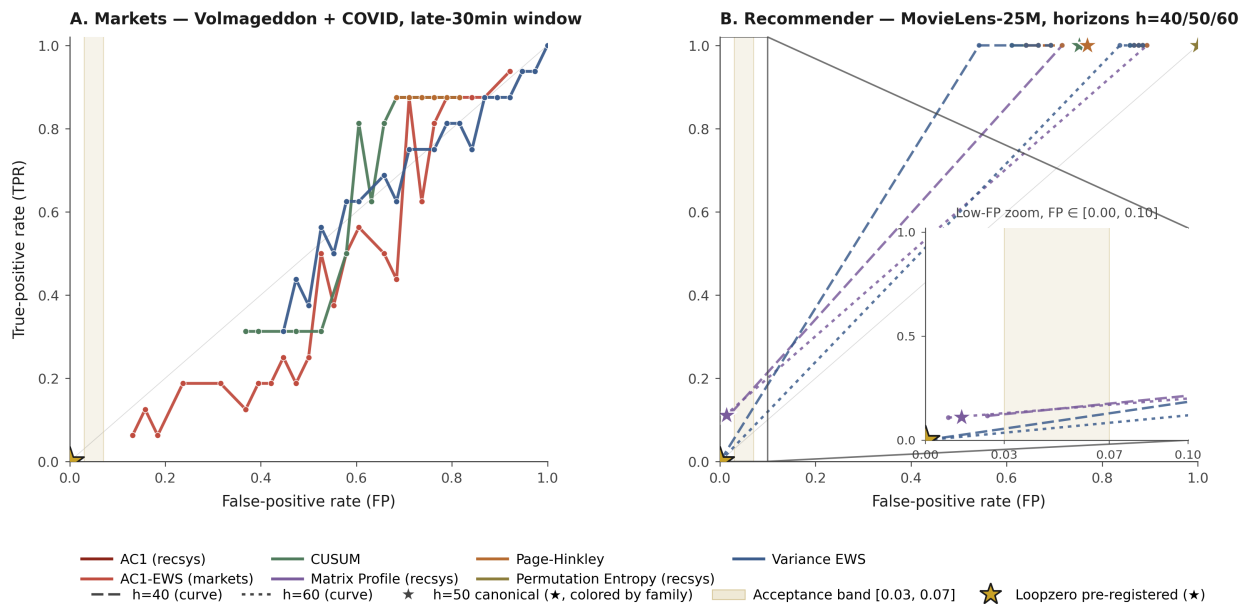


Figure 7. Comparator operating points relative to the locked equal-FP band $[0.03, 0.07]$. (A) Markets (Volmageddon + COVID, late-30min window; $n=38$ controls + 16 events): four fast families overfire above the band; slow families (matrix profile, permutation entropy) fail at the data-availability gate on this late-window panel because their min-length requirement reduces usable $n_control_units$ below band reachability (these families are evaluated on the full-window benchmark in Figure 4). (B) Recommender (MovieLens-25M; 40,339 user clusters per horizon panel; per-horizon event/control splits — $h=40$: $n_control=6,562 / n_event=33,777$; $h=50$ canonical: $n_control=4,755 / n_event=35,584$; $h=60$: $n_control=3,996 / n_event=36,343$) at horizons $h=40$ (long dash), $h=50$ (★ canonical), $h=60$ (short dash): all six families miss the band; inset shows the low-FP region $[0.0, 0.10]$ with the matrix-profile near-miss at $FP \approx 0.014$. Gold ★ marks the pre-registered Loopzero conservative operating point ($q=95, k=3$) at ($FP \approx 0, TPR \approx 0$); this is a single deliberately strict configuration, not the achievable Loopzero envelope. The achievable Loopzero envelope across the extended envelope-boundary sensitivity grid is reported in the *Envelope-boundary matched-FP comparison* subsection. No tested comparator configuration achieves an accepted operating point under the locked equal-FP contract.

Envelope-boundary matched-FP comparison Figure 7 anchors the cross-benchmark synthesis at a single deliberately strict Loopzero operating point ($q = 95$, $k = 3$) at ($FP \approx 0$, $TPR \approx 0$). To characterize the achievable Loopzero envelope rather than this single anchor, we extended the pre-registered sensitivity grid to $q \in \{50, 60, 70, 75, 80, 85, 90, 95, 99\}$ (Methods), holding $k = 3$ fixed at the canonical primary value. At each panel, Loopzero’s envelope-boundary operating point is the maximum control_fp achieved across the extended q -grid; comparator families are then reported at the linearly interpolated TPR at the same boundary FP, or marked as a structural non-overlap where the family’s frozen calibration grid does not bracket Loopzero’s boundary (Table 2).

On the markets benchmark, Loopzero’s envelope boundary at $k = 3$ is ($FP = 0.237$, $TPR = 0.188$), reached at $q = 50$. Of the four markets comparator families that satisfied data-availability gating in the $[0.03, 0.07]$ equal-FP contract evaluation, only ac1_ews has any operating point at or below $FP = 0.237$; at that exact rate, the ac1_ews and Loopzero quantile detector operating points are identical. In integer alarm counts (Supplementary Table S3), both methods alarm on exactly 9 of 38 controls and detect exactly 3 of 16 events at this matched anchor — alarm-set equivalence rather than a rate coincidence forced by the discrete FP grid (control units quantize FP to multiples of $1/38 \approx 0.0263$). The remaining three markets families (cusum, page_hinkley, variance_ews) have minimum operating points strictly above Loopzero’s envelope-boundary FP — they operate in a higher-FP regime than Loopzero across the extended grid.

On the recommender benchmark, the pattern is sharper. Loopzero’s envelope boundary at $k = 3$ sits at $FP = 0.0148$ ($h = 40$), 0.0023 ($h = 50$ canonical), and 0.000501 ($h = 60$). Of the six standard EWS comparator families calibrated on the recommender benchmark, four (ac1, cusum, page_hinkley, matrix_profile) have minimum operating points that exceed Loopzero’s envelope boundary at $h = 40$ and $h = 60$; at $h = 50$, Loopzero’s boundary FP (0.0023) lies below the comparator calibration grids’ coverage, so $h = 50$ is excluded from this cross-horizon comparison (Table 2, Supplementary Table S3). One family (permutation_entropy) has only a single unique FP per horizon in its frozen calibration grid — insufficient coverage to support envelope comparison. Only one family (variance_ews) has any envelope overlap with Loopzero’s quantile detector, and that overlap is itself qualified by the comparator’s pre-registered grid coverage: at $h = 40$, variance_ews’s frozen calibration matrix has a 3559-alarm gap directly across Loopzero’s anchor of 97 alarms (Supplementary Table S3); at $h = 60$, the equivalent gap is 3345 alarms across Loopzero’s anchor of 2 alarms. The linear-interpolated TPR values for variance_ews at Loopzero’s envelope-boundary FP — 0.027 at $h = 40$ and 0.0006 at $h = 60$ — are accordingly estimates across these calibration-grid gaps rather than measurements at the boundary FP.

The headline structural finding is therefore not interpolation-dependent. Of the six standard EWS comparator families calibrated on the recommender benchmark at the canonical $k = 3$, four operate in a strictly higher false-positive regime than Loopzero’s quantile detector across all 9 q values of the extended envelope-boundary sensitivity grid at $h = 40$ and $h = 60$. One has insufficient calibration coverage to support envelope comparison. Only variance_ews has any calibration coverage in Loopzero’s operating regime — coverage qualified by a 3559-alarm gap on $h = 40$ (3345 on $h = 60$) directly across Loopzero’s envelope-boundary anchor. The envelope-boundary contract therefore identifies a structural property of standard EWS comparator literature on the recommender benchmark. The operating regimes of the canonical comparator families do not extend into the false-positive regions reached by a percentile-based recursive-collapse detector across the extended envelope-boundary sensitivity grid evaluated here.

Table 2. Envelope-boundary matched-FP comparison at the canonical $k = 3$. Panels:

markets (n=38 controls + 16 events) and recommender at horizons h=40, h=50, h=60 (40,339 user clusters per horizon panel; per-horizon event/control splits — h=40: n_control=6,562 / n_event=33,777; h=50 canonical: n_control=4,755 / n_event=35,584; h=60: n_control=3,996 / n_event=36,343). Loopzero’s operating envelope boundary across the extended envelope-boundary sensitivity grid ($q \in \{50, 60, 70, 75, 80, 85, 90, 95, 99\}$) on each panel. Comparator families with envelope overlap are reported at the linearly interpolated TPR at Loopzero’s boundary FP; non-overlapping families have minimum operating points exceeding Loopzero’s boundary FP. Alarm-count detail and breakpoint context in Supplementary Table S3.

Panel	Loopzero envelope boundary at k=3	Overlapping comparator (TPR at boundary FP)	Non-overlapping families
Markets	FP = 0.2368, TPR = 0.188 (q = 50)	ac1_ews: 0.188 (exact match; alarm-set equivalent at 9/38 controls, 3/16 events)	cusum, page_hinkley, variance_ews: minimum FP > 0.237
Recsys h=40	FP = 0.0148, TPR = 0.092 (q = 50)	variance_ews: 0.027 (interpolated across 3559-alarm calibration gap)	ac1, cusum, page_hinkley, matrix_profile: minimum FP > 0.0148; permutation_entropy: insufficient grid coverage
Recsys h=50	FP = 0.0023, TPR = 0.075 (q = 50)	— (no comparator breakpoint at this boundary FP)	—
Recsys h=60	FP = 0.000501, TPR = 0.055 (q = 50)	variance_ews: 0.0006 (interpolated across 3345-alarm calibration gap)	ac1, cusum, page_hinkley, matrix_profile: minimum FP > 0.0005; permutation_entropy: insufficient grid coverage

Discussion

The scientific claim of the paper is deliberately minimal: collapse in recursive systems admits a formally specified observable predicate with an explicit claim boundary, and under equal-false-positive fairness, tested standard comparator configurations did not recover the same admissible operating behavior on canonical benchmarks. The significance lies in the conjunction. A formal obstruction motivates a conditional measurable pre-collapse signature; under matched-false-positive fairness against a broad comparator suite, that directional signature is recovered on the canonical benchmarks and no tested comparator configuration achieved an accepted operating point. Unlike threshold-tuned detectors, the empirical program is explicitly

falsifiable under a fixed equal-false-positive contract.

Methodological positioning. The matched-false-positive contract is conceptually rooted in operating-point selection on ROC curves and is equivalent in spirit to Neyman–Pearson hypothesis testing evaluated at a chosen specificity. In sequential change-point detection, family-appropriate calibration of CUSUM and Page–Hinkley statistics is conventionally done via expected average run length under the null (ARL_0 ; Page, 1954); the locked equal-false-positive band $[0.03, 0.07]$ is the finite-sample matched-FP analog adapted for recursive-collapse benchmarks where control-unit counts are bounded. The contribution is not the invention of false-positive control but its disciplined application: a prespecified band, frozen public-artifact benchmarks with event labels fixed independently of witness computation and comparator calibration, and reported outcomes including non-acceptance.

Relation to early-warning-signal literature. The framework is distinct from the classical critical-transitions early-warning-signal (EWS) framework. The canonical EWS suite — increasing variance, lag-1 autocorrelation, and critical slowing down near bifurcations (Scheffer et al., 2001, 2009) — operates on stationary-noise dynamical systems approaching a tipping point and has documented false-positive vulnerabilities under non-stationary forcing (Boettiger & Hastings, 2012a, 2012b). The matched-FP contract is the methodological response to the family-comparability problem identified by that limitations literature. The empirical bridge tested here is conceptually distinct: G , p , and δ operationalize a recursive no-progress obstruction rather than a noise-amplification signature near a bifurcation. Loopzero is therefore not a replacement for critical-slowness detection in dynamical systems near bifurcations; it tests a different conditional bridge under an explicit alert-budget contract, on benchmarks where recursive feedback structure is the primary feature.

Falsifiability and current verdict. The framework is explicitly falsifiable. It would be weakened if (i) externally defined collapse events occurred without the predicted directional $G/p/\delta$ pattern in the pre-collapse window; (ii) control units showed the same pattern without subsequent collapse events; (iii) tested standard comparators recovered accepted operating points under the locked false-positive contract on the canonical benchmarks; or (iv) Loopzero’s pre-registered quantile detector recovered accepted operating points on benchmarks where the bridge signature was absent. Across the canonical benchmarks, the directional witness pattern is recovered in the pre-collapse windows; no tested comparator configuration achieves an accepted operating point; and Loopzero’s pre-registered quantile detector itself does not achieve an accepted operating point with nonzero event recovery on any panel. This pattern is consistent with the framework as a falsifiable empirical program rather than a completed operational detector.

Domain-specific restraint. The recommender branch (MovieLens-25M offline deterministic replay) provides a corroborating second flagship benchmark. Offline recommender evaluation is subject to selection biases relative to deployed-system behavior (Schnabel et al., 2016); results test bridge survival under controlled deterministic replay rather than predicting online user response. Adjacent-horizon sensitivity preserves the comparator non-recovery result at $h=40$ and $h=60$ while the bridge degrades asymmetrically (Supplementary Table S2), supporting a corroborating benchmark with bounded sensitivity rather than unqualified invariance.

The markets branch provides bounded real-world corroboration. The segmented benchmark is externally grounded, the band is reachable, the comparator suite is broad, and no tested fast or slow configuration admits an accepted operating point. Inferential strength is limited by small event-scenario count ($n=2$ event clusters) and within-event dependence; cluster-aware bootstrap

at scenario grain (Supplementary Table S4) is reported as a dependence-sensitivity diagnostic, not as primary inference. Wild cluster bootstrap (Cameron, Gelbach & Miller, 2008) is the methodologically appropriate calibration in this small-cluster regime and is deferred to follow-up work.

The third domain — recursive LLM training-loop collapse (Shumailov et al., 2024) — was evaluated as a secondary directional-consistency check rather than a matched-FP benchmark: all three witnesses moved in the predicted direction across the collapse transition, with graded predictions on collapse severity and preservation regime also visible. Matched-FP comparator evaluation in this domain is deferred.

Limitations and forward path. Witness construction is still domain-adapted. Comparator scope could expand. The bridge criterion, although explicit and falsifiable here, remains empirical rather than an identification result. The threshold-path envelope-boundary analysis shows that Loopzero’s quantile detector operates in a structurally lower-FP regime than four of the six standard recommender-benchmark comparator families across the extended envelope-boundary sensitivity grid at $h = 40$ and $h = 60$ — a finding independent of detector tuning. The directional bridge result and this envelope-boundary structural finding remain distinct from the stronger binary-acceptance claim, which the pre-registered ($q=95$, $k=3$) configuration does not satisfy and which remains open for future detector development at parameter regimes outside the present pre-registered grid. A per-witness effect-size decomposition (Figure 6) indicates that no single witness carries the canonical result. At the pre-registered horizon $h=50$, G , p , and δ each align in the predicted direction with BCa intervals clear of null. Diversity contributes the largest single magnitude there: Cohen’s $d \approx -0.17$, versus $\approx +0.10$ for G and $\approx +0.08$ for p , so diversity contraction is the strongest individual witness on the canonical panel rather than a passenger. The witnesses also trade off across horizons. At $h=40$, G runs counter to prediction ($d \approx -0.21$) while p and δ remain aligned with intervals clear of null. At $h=60$, G strengthens ($d \approx +0.33$) while the p and δ intervals relax to null. On the markets benchmark the segment-grain effect sizes are individually modest with intervals spanning null, consistent with the localized late-window character of the markets bridge. This decomposition describes relative per-witness contribution and is not a detector ablation; component-level necessity of G , p , and δ through full ablations is reserved for follow-up work.

The next scientific step is not rhetorical expansion but stress-testing: additional domains under full matched-FP comparator evaluation, external replication, intervention logic, and broader comparator classes.

Materials and Methods

The paper combines a Lean-formalized minimal obstruction (de Moura & Ullrich, 2021; The mathlib Community, 2020) with empirical witness construction over gain, recursive persistence, and diversity. Empirical evaluation is performed under a locked equal-false-positive contract, so detector families are compared at the same alert budget rather than at arbitrary thresholds. Bridge satisfaction is operationally defined as follows. Under the prespecified pre-collapse window, event-unit summaries of G are higher than control-unit summaries, p maintains its non-relaxation property, and event-unit summaries of δ are lower than control-unit summaries. Bridge non-satisfaction is defined as failure of any of these conditions. The remaining subsections specify the analysis layers and claim status, domain inclusion criteria, per-domain data provenance and benchmark construction, comparator scope, the envelope-boundary matched-FP contract, cluster-robust sensitivity, the BCa bootstrap procedure, artifact availability with axiom audit,

offline-evaluation limitations, and reproducibility anchors.

Analysis layers and claim status. The empirical and formal contributions of this paper are organized into the following analysis layers; each is reported under an explicit claim status to prevent inference inflation across layers.

Layer	Purpose	Pre-registered?	Claim status
A0	Lean-formalized recursive no-progress obstruction (collapse_via_progresscycle_public, telemetry_bridge_obstruction_public)	Frozen Lean artifact	Formal claim boundary only; does not verify empirical telemetry or measurement map
A1	Loopzero’s primary quantile detector at canonical configuration (q = 95, k = 3) under locked equal-FP band [0.03, 0.07]	Yes (canonical configuration pre-declared)	Non-accepted on both benchmarks (FP = 0.000, event alarm rate = 0.000)
A2	Envelope-boundary threshold-path analysis over extended quantile grid $q \in \{50, 60, 70, 75, 80, 85, 90, 95, 99\}$	Extended sensitivity grid	Exploratory structural analysis; not a primary detector claim
A3	G/p/ δ witness Cohen’s d effect sizes with cluster-aware BCa intervals	Descriptive	Directional alignment and magnitude summary; effect sizes small at h=50 canonical and weakening for h=60 on p and δ
B1	Negative recommender controls (shuffled-timestamp, popularity-only, random, matrix-factorization, sequential)	Not yet run	Deferred to v1.1; required for recursive-recommender mechanism specificity

Layer	Purpose	Pre-registered?	Claim status
B3	Scenario-grain markets cluster sensitivity (n = 7 clusters; Supplementary Table S4)	Sensitivity	Dependence-sensitivity diagnostic at n = 2 event clusters; intervals not reliable conservative inferential intervals; wild cluster bootstrap deferred

Acceptance under the locked false-positive contract is a property of A1 only. A2 results are reported to characterize the threshold-path structure of the pre-registered detector grid and the comparator grids; they are not used to claim operating-point acceptance. A3 effect-size summaries support the directional bridge but are not equivalent to detector acceptance.

Domain inclusion criteria. The matched false-positive framework requires three operational criteria of a candidate domain. First, a frozen public-artifact benchmark with event labels fixed independently of the witness computation and comparator calibration — either externally defined real-world events (e.g., the markets-domain intervention windows used here) or benchmark-defined held-out failures under frozen rules (e.g., the MovieLens-25M held-out frontier failures used here), in both cases not generated by the analytical framework being tested. Second, sufficient control units to make the prespecified equal-false-positive band $[0.03, 0.07]$ reachable on the control-unit FP grid. Third, feasible witness construction: a measurement map from system state to a preorder under which the G, p, δ witness triad is observable. Two recursive-feedback domains satisfy all three criteria and are adopted as canonical matched-FP benchmarks: a markets domain (volmageddon 2018 and COVID MWCB 2020) and a recommender-system domain (MovieLens-25M offline deterministic replay). The recursive language-model training-loop domain (Shumailov et al., 2024) is retained as a secondary directional-consistency check only. Published per-generation trajectories support directional witness analysis, but raw trajectories at the scale required for matched-FP comparator evaluation are not publicly available; matched-FP evaluation in this domain is deferred to follow-up work. Other recursive-feedback domains were considered but not adopted. Synthetic bandit simulators (toy bandits, LinUCB, ϵ -greedy) were excluded because the collapse criterion is part of the simulator specification, creating circularity under matched-FP evaluation. A cognition domain (n-back and digit-span working-memory tasks) was excluded because no public dataset at scale provides externally validated working-memory-failure labels suitable for matched-FP comparator evaluation. Cultural and social-media systems (Wikipedia edit dynamics, Reddit thread evolution) were excluded because candidate “echo-chamber” or “topic-saturation” labels co-occur with the witness pattern by construction (topic-entropy floor functioning as both label and δ -proxy), creating measurement circularity.

Markets data provenance. Minute-bar OHLCV data for the six US-listed instruments SPY, QQQ, IWM, VXX, UVXY, SVXY across the canonical 2017–2020 window — covering both the XIV/SVXY February 2018 Volmageddon implosion and the March 2020 COVID-era Level 1 market-wide circuit breaker triggers — were obtained via the Alpaca Markets historical market data API (<https://alpaca.markets/>, accessed 2025). Under the vendor’s terms of service, raw minute bars are not redistributed alongside this artifact; the ingestion and preprocessing pipeline is maintained in an upstream private repository and reproduces minute bars from an Alpaca

subscription. Per-segment derived ingredient packets containing log returns, absolute returns, intraday stress flags, breadth indicators, and Loopzero telemetry features (G , p , δ) at one-minute resolution are released in this artifact at `results/rendered/equity_dislocation_family/intraday_v2_ingredient_packet/`; each canonical event window (`volmageddon_2018_xiv`, `covid_mwcb_2020_03_18`) and matched control window is materialized as a 54-column packet over the 16-hour intraday window (typically 944 rows per segment). Event-window definitions, trigger semantics, and the canonical late-30-minute summary slice follow the post-event analyses cited in the references (Augustin et al., 2021; NYSE Market-Wide Circuit Breaker Working Group, 2021). The matched-FP comparator calibration runs against the frozen `markets_comparator_merged_state_v2` (Supplementary Table S5). The public-reproducibility scope of the markets benchmark is at the derived-packet level: the released ingredient packets contain all telemetry features (G , p , δ , breadth indicators, stress flags) and event/control window labels required for any researcher to independently re-run the matched-FP contract against the frozen comparator calibration state. Bottom-up reconstruction from raw minute bars requires an Alpaca Markets subscription under vendor terms; this scope partition — derived telemetry public, raw vendor feed private — is standard for vendor-licensed market data and does not affect verifiability of the matched-FP comparator-acceptance results reported in this paper.

Markets benchmark construction. The canonical segmented markets benchmark `volmageddon_covid_public_v2` (canonical Loopzero configuration `cfg_001339`) was constructed from a curated set of intraday packet ingredients drawn from minute-bar data for six US-listed instruments — SPY, QQQ, IWM, VXX, UVXY, and SVXY — covering the Volmageddon dislocation (February 2018; Augustin et al., 2021) and the March 2020 COVID market-wide circuit-breaker cluster (NYSE MWCBC Working Group, 2021). Each canonical packet contains preprocessed Loopzero telemetry (G , p , δ) for one underlying time series; non-canonical configurations were excluded to avoid duplicated session units. Each packet was sliced into 120-minute time-window segments (minimum 60 retained minute-bars per segment), and each (slice \times segment) pair became one comparator unit. Event/control assignment was made by membership of the slice identifier in a prespecified list of canonical event identifiers (e.g., `volmageddon_2018_xiv`, `covid_mwcb_2020_03_18`), with hard negative controls drawn from non-event slices over the same instrument universe. Under this construction, 38 control units and 16 event units were retained, yielding an FP grid step of $1/38 = 0.026316$. Calibration semantics are full-benchmark with per-unit rolling-quantile thresholds and no held-out partition. Because each segment is treated as an independent comparator unit during calibration, intra-event correlation under shared market-wide stress is a dependence limitation addressed at scenario grain in the Cluster-robust sensitivity subsection (B3); wild cluster bootstrap remains for follow-up work.

Recommender benchmark construction. The canonical recursive recommender benchmark `movielens25m_recursive_frontier_public_v1` was constructed from the public MovieLens-25M dataset (<https://grouplens.org/datasets/movielens/25m/>). Per-user trajectories were sorted chronologically and reduced to one episode per user. Each episode was replayed under a deterministic item-item collaborative-filtering engine with a warm-start prefix and a held-out positive frontier; collapse was defined as failure to recover held-out positive-frontier items under frozen benchmark rules. The canonical horizon was 50 recursive update steps; adjacent horizons of 40 and 60 steps were tested for bridge-sensitivity robustness. Under the canonical 50-step construction, 40,339 user-level units satisfied inclusion criteria, of which 35,584 were event units (collapse occurred within the canonical horizon) and 4,755 were control units (collapse did not occur within the canonical horizon), yielding an FP grid step of $1/4755 \approx 0.0002103$. Comparator families were evaluated against a derived per-user benchmark series,

`miss_run_fraction`, capturing recursive frontier-miss runs over the canonical horizon. Each user is treated as an independent unit in calibration. Full parameter specification — including the positive-rating threshold, frontier size, warm-start prefix length, item-item engine configuration, and leakage-prevention rules — is recorded in the canonical manuscript freeze state (`movielens25m_recursive_frontier_public_v1_manuscript_freeze_state.json`), with construction details documented in the Supplementary Materials.

Comparator scope and exclusions. The six comparator families evaluated under the matched-FP contract — variance EWS and lag-1 autocorrelation AC1 (Dakos et al., 2012), CUSUM (Page, 1954), Page-Hinkley (Page, 1954), matrix profile (Yeh et al., 2016), and permutation entropy (Bandt & Pompe, 2002) — are the established detection-theoretic and early-warning-signal baselines in the critical-transitions and online change-point literature for the recursive-collapse setting. Four additional comparator families are out of scope for this version with explicit rationale. (i) Generalized likelihood ratio (GLR) tests require parametric distributional assumptions on the pre-collapse generative process that the matched-FP contract is designed to avoid, and are reserved for follow-up work with non-parametric extensions. (ii) Bayesian online change-point detection is computationally prohibitive at the canonical recsys grain ($n = 40,339$ user clusters \times 50-step horizon); Rao-Blackwellized acceleration is deferred to follow-up work. (iii) Supervised sequence classifiers require labeled training data, violating the unsupervised early-warning scope of the matched-FP framework. (iv) Transformer-based anomaly detectors and modern foundation-model detectors are within scope methodologically but require pre-training corpora whose collapse-content composition is not auditable, creating a circularity risk that a follow-up protocol can address via self-supervised representation baselines decoupled from collapse labels. The matched-FP framework is family-agnostic: any detector returning a per-unit alarm decision can be evaluated under the same locked contract; researchers extending the comparator suite should follow the pre-registered grid protocol and frozen calibration freeze pattern at `results/frozen/comparators/`.

Envelope-boundary matched-FP contract. Loopzero’s pre-registered sensitivity grid ($q \in \{90, 95, 99\}$; $k \in \{1, 3, 5\}$) was extended downward to $q \in \{50, 60, 70, 75, 80, 85, 90, 95, 99\}$ for envelope-boundary threshold-path evaluation. The extension stays within the detector’s percentile design space and stops at $q = 50$ — the semantic boundary of percentile-based threshold detection, below which a trigger sits at or beneath the reference median. The canonical primary configuration ($q = 95, k = 3$) is unchanged. Standard EWS comparator families operate from their frozen pre-registered calibration matrices; we do not extend these grids post-hoc, since doing so would either compromise byte-exact reproducibility of the frozen state or constitute research-grade extension outside the original method papers’ recommendations. At each panel and at the canonical $k = 3$, Loopzero is reported at the maximum `control_fp` it achieves across the extended q -grid (its operating envelope boundary); each comparator family is reported at the linearly interpolated TPR at the same boundary FP where the family’s calibration grid brackets that FP, or marked as a structural non-overlap otherwise. A companion sensitivity analysis re-expresses this comparison in integer alarm counts, surfacing where discrete FP space forces rate coincidences into literal alarm-count equivalences and where linear interpolation fills quantitative gaps in the frozen pre-registered calibration grids. Full computation is at `analysis/20_compute_a2_threshold_path.py` and `analysis/21_compute_a2_alert_count_exact.py`, with outputs in `results/calibrated/`.

Cluster-robust sensitivity at scenario grain. The markets benchmark’s matched-control design induces a paired cluster structure (2 event scenarios totaling 16 segments; 5 control scenarios

totaling 38 segments). To verify that the markets effect-size analysis is robust to within-scenario dependence beyond the segment-level resampling reported in Supplementary Table S2, we re-ran the cluster-aware bootstrap with cluster grain shifted from segment-level ($n = 54$ segments) to scenario-level ($n = 7$ clusters). Point estimates are identical across cluster grains; only the bootstrap CIs change. At $n = 2$ event clusters the standard cluster bootstrap is in the small-cluster regime where Cameron, Gelbach, and Miller (2008) documented downward variance bias relative to wild cluster bootstrap; we treat the scenario-grain bootstrap as sensitivity rather than primary inference, with wild cluster bootstrap reserved for follow-up work. Full cluster composition and per-cell results are reported in Supplementary Table S4.

BCa bootstrap procedure. Bias-corrected and accelerated (BCa) intervals follow Efron (1987). The bias-correction constant z_0 is computed as the inverse normal CDF of the proportion of bootstrap replicates below the point estimate. The acceleration constant \hat{a} is computed via jackknife resampling at the cluster grain (segment-level for markets, user-level for recsys). Separately, bootstrap replicates that are degenerate (e.g., zero variance from same-scenario cluster resamples) are finite-filtered, and the per-cell `n_degenerate` count is recorded (Supplementary Table S4 reports one such case at 2 of 10,000 iterations for the p|Glass’s d cell at B3 scenario grain). Across all 27 recsys cells at $n = 40,339$, $|\text{BCa} - \text{percentile}| < 0.01$ on every endpoint, consistent with BCa’s $O(1/\sqrt{n})$ second-order correction theory; the recsys BCa report is therefore primarily for procedural consistency with markets, where the right-skewed bootstrap distribution at finite n favors BCa as the more honest read.

Artifact availability. The Lean keeper surface — `no_progress_cycle_public`, `no_progress_kcycle_public`, `collapse_via_progresscycle_public`, `TelemetryState`, `telemetry μ` , `telemetry_bridge_obstruction_public`, and `no_telemetry_forbidden_cycle_public` — is publicly archived at <https://github.com/davidmullett/loopzero-paper-public> (release tag `lean-v1.0`) and is reproducible under Lean v4.30.0-rc2 with Mathlib at commit `3ba1ec58ec69cd649b9e5c61485a98d1dd37a00f`. The build runs cleanly under `lake build`. An axiom audit verifies that the three obstruction theorems (`no_progress_cycle_public`, `no_progress_kcycle_public`, `collapse_via_progresscycle_public`) compile without any axiom dependencies, while the two telemetry-bridge theorems (`telemetry_bridge_obstruction_public`, `no_telemetry_forbidden_cycle_public`) depend only on the standard Mathlib trusted base (`propext`, `Classical.choice`, `Quot.sound`). No non-standard axioms appear in the keeper surface.

Offline-evaluation limitations. The MovieLens-25M recommender benchmark is subject to the standard offline-evaluation biases of explicit-rating datasets. Ratings are missing-not-at-random: items receive ratings conditional on a user having chosen to consume them, so the observed-rating distribution is not representative of the user’s true preference distribution. Without logged exposure data, item-exposure probabilities cannot be inferred (Schnabel et al., 2016; Chaney et al., 2018), and popularity bias affects both the candidate set and the held-out frontier evaluation (Fleder & Hosanagar, 2009; Jiang et al., 2019; Mansoury et al., 2020). The benchmark constructed here is therefore explicitly framed as a deterministic offline replay over a frozen public dataset, not as evidence about deployed recommender systems exposed to live user feedback. Mechanism-specificity controls — random recommender, popularity-only, matrix-factorization, sequential, and shuffled-timestamp baselines — are deferred to v1.1 and are required for claims about recursive-recommender collapse mechanism specifically, as distinct from the recursive-replay frontier-failure pattern reported here.

Reproducibility anchors. All empirical results in this paper are anchored to immutable frozen artifacts indexed by SHA-256 hash. The recommender benchmark uses the `movielens_`

recursive_replay_engine v1.0.0 (family item_item_collaborative_filtering, engine hash 56c1cff225d60c09) operating under contract SHA-256 2e256b255a7f074c1516d70315ebb216241a4a7e8aba2db88b194417705fd71d; all three tested horizons (h=40, h=50 canonical, h=60) are generated parametrically from this engine and contract. The upstream MovieLens-25M archive is the canonical GroupLens release (ml-25m.zip, archive SHA-256 8b21cfb7eb1706b4ec0aac894368d90acf26ebdfb6aced3ebd4ad5bd1eb9c6aa, MD5-verified against the official GroupLens checksum at <https://files.grouplens.org/datasets/movielens/ml-25m.zip.md5>; raw-input provenance manifest at results/manifests/movielens25m_recursive_frontier_public_v1__raw_input_provenance.json). Frozen-state freeze-manifests for each empirical component are listed in Supplementary Table S5; each frozen directory additionally contains a LOCK_NOTE.md documenting the scientific and editorial scope of that freeze. The three recsys horizon panels (h=40, h=50 canonical, h=60) are byte-exact deterministic derivations from the single benchmark freeze state and contract under horizon parameter $h \in \{40, 50, 60\}$; given identical (freeze_state, contract, h), the engine produces identical outputs. Horizon-spanning coverage is anchored by the recsys horizon sensitivity manifest (Supplementary Table S5).

Supplementary Materials

Supplementary materials accompanying this article comprise:

- Supplementary Figure S1: Fast-family segmentation and band sensitivity on the canonical markets benchmark
- Supplementary Table S2: Effect sizes with bootstrap 95% confidence intervals
- Supplementary Table S3: Alert-count exact-matching sensitivity check
- Supplementary Table S4: Cluster-robust sensitivity at scenario grain (markets benchmark)
- Supplementary Table S5: Reproducibility anchor hashes

These are submitted as an arXiv ancillary file and are also available at the public repository (<https://github.com/davidmullett/loopzero-paper-public>).

Funding

This research was conducted by the author as an independent investigator and received no external funding.

Author contributions

D.M. conceived the study, developed the theoretical framework, implemented all software and analyses, and wrote the manuscript.

Competing interests

The author declares no competing interests.

Data and code availability

All public analysis code, derived telemetry packets, frozen calibration outputs, and reproducibility anchors needed to reproduce the reported analyses from the released artifacts are available at <https://github.com/davidmullett/loopzero-paper-public>; raw vendor market data and the

upstream ingestion/preprocessing repository are not redistributed (see Markets data provenance). The repository includes:

- All analysis scripts used to generate every figure and table (`analysis/`)
- Frozen calibration outputs and operating-point data (`results/`)
- Benchmark construction code for the markets and recommender domains
- This manuscript’s source and rendered outputs (`manuscript/`)

External datasets used:

- MovieLens-25M is publicly available from GroupLens (<https://grouplens.org/datasets/movielens/>)
- The Shumailov et al. (2024) data shown in Figure 5 was digitized from the published figures of the cited Nature paper

Reproducibility anchors documented in Materials and Methods include Loopzero’s pre-registered detector configuration (`q_G=95`, `q_p=95`, `q_delta=5`, `k=3`), the equal-false-positive contract band $[0.03, 0.07]$, the analysis seeds (`RANDOM_SEED=42` for A3 segment-grain analyses, `RANDOM_SEED_B3=43` for B3 scenario-grain analyses), and the bootstrap iteration count (10,000 per cell).

Figure and Table Legends

Supplementary Figure S1. Fast-family segmentation and band sensitivity on the canonical markets benchmark. No fast-family comparator was accepted at 60-, 120-, or 180-minute segmentation under the prespecified equal-false-positive band $[0.03, 0.07]$. Under widened post-processing bands with upper cutoff 0.08, acceptance appeared only for the 60-minute AC1 configuration; the canonical 120-minute and 180-minute segmentations remained non-accepted across all tested bands.

Supplementary Table S2. Effect sizes with bootstrap 95% confidence intervals. Per-witness Cohen’s d , Glass’s d , and rank AUC at each benchmark/horizon (4 benchmarks \times 3 witnesses \times 3 effect measures = 36 cells), with both BCa-adjusted and percentile bootstrap confidence intervals from cluster-aware resampling (10,000 iterations). Markets uses segment-level resampling ($n=38$ controls + 16 events); recommender (all horizons) uses user-level resampling ($n = 40,339$ user clusters). Canonical $h=50$ group is bolded throughout. A sensitivity section flags cells where BCa and percentile CI endpoints differ by ≥ 0.05 (markets p-witness cells only — the bootstrap distribution is right-skewed at low n , and BCa is the more honest read there). Full numerics rendered deterministically by `analysis/17_render_a3_supplementary_table_s2.py` from the per-cell bootstrap output at `results/rendered/effect_sizes/a3_effect_sizes_full.csv`.

Supplementary Table S3. Alert-count exact-matching sensitivity check. Re-expression of the envelope-boundary matched-FP comparison (main-text Table 2) in integer alarm counts. For each panel at the canonical $k = 3$, Loopzero is reported at its envelope-boundary alarm counts (`n_control_alarmed`, `n_event_alarmed`); each comparator family’s frozen pre-registered calibration grid is searched for the operating point with the nearest `n_control_alarmed` value, with status classified as `exact_match` (comparator has an operating point at Loopzero’s exact alarm count), `bounded_gap` (Loopzero’s alarm count falls between two adjacent comparator operating points, with `gap_width_n_control` quantifying the calibration coverage gap), `no_overlap_above` (all comparator operating points have higher alarm counts), or `insufficient_data`. On the

markets benchmark, `ac1_ews` exhibits `exact_match` at Loopzero’s envelope-boundary anchor: both methods alarm on exactly 9 of 38 controls and detect exactly 3 of 16 events. On the recommender benchmark, `variance_ews` exhibits the widest bounded gaps across Loopzero’s envelope boundary: 3559 alarms at $h = 40$ (Loopzero at 97 of 6562 controls) and 3345 alarms at $h = 60$ (Loopzero at 2 of 3996 controls), in each case with the upper-bound comparator operating point detecting all panel event units ($\text{TPR} = 1.0$). Full numerics rendered by `analysis/21_compute_a2_alert_count_exact.py` from frozen calibration data at `results/rendered/a4_roc_lowfp/a4_roc_data.parquet` and operating-point data at `results/rendered/bridge/a1_loopzero_operating_points{, _h40_h60}.csv`.

Supplementary Table S4. Cluster-robust sensitivity at scenario grain (markets benchmark). Per-witness effect sizes (Cohen’s d , Glass’s d , rank AUC) on the markets benchmark at the A3 segment grain ($n = 54$ segments) and the B3 scenario grain ($n = 7$ clusters: 2 event scenarios — `volmageddon_2018_xiv` with 8 segments and `covid_mwcb_2020_03_18` with 8 segments; 5 control scenarios — `covid_noncollapse_2020_03_11` with 8 segments, `volmageddon_control_2018_01_29` with 8 segments, `volmageddon_control_2018_02_08` with 8 segments, `covid_noncollapse_2020_03_13` with 7 segments, `volmageddon_control_2018_01_25` with 7 segments). Bootstrap iterations: 10,000 per cell; CI level: 0.95; RNG seed for scenario grain: 43 (distinct from A3 segment grain seed: 42). For p|Glass’s d at scenario grain, 2 of 10,000 iterations produced degenerate samples (control SD ≈ 0 from same-scenario cluster resamples); finite-filter applied to remaining 9,998 iterations. All other 8 cells: `n_degenerate` = 0. Scenario-grain CIs are reported as sensitivity, not primary inference; the segment-grain baseline (Supplementary Table S2) remains the primary report.

Supplementary Table S5. Reproducibility anchor hashes. Freeze-manifest SHA-256 hashes for the empirical components of this paper, plus the recommender engine identifiers (`engine_hash` 56c1cff225d60c09, contract SHA-256 2e256b255a7f074c1516d70315ebb216241a4a7e8aba2db88b194417705fd71d) and the upstream MovieLens-25M archive hash (8b21cfb7eb1706b4ec0aac894368d90acf26ebdfb6aced3ebd4ad5bd1eb9c6aa, MD5-verified against the GroupLens official checksum). Full table is in the Supplementary Materials.

References

- Augustin, P., Cheng, I.-H. and Van den Bergen, L. (2021). Volmageddon and the failure of short volatility products. *Financial Analysts Journal*. <https://doi.org/10.1080/0015198X.2021.1913040>
- Bandt, C. and Pompe, B. (2002). Permutation entropy: a natural complexity measure for time series. *Physical Review Letters*, 88, 174102. <https://doi.org/10.1103/PhysRevLett.88.174102>
- Boettiger, C. and Hastings, A. (2012a). Early warning signals and the prosecutor’s fallacy. *Proc. Royal Society B*. <https://doi.org/10.1098/rspb.2012.2085>
- Boettiger, C. and Hastings, A. (2012b). Quantifying limits to detection of early warning for critical transitions. *Journal of the Royal Society Interface*. <https://doi.org/10.1098/rsif.2012.0125>
- Brunnermeier, M.K. and Pedersen, L.H. (2009). Market liquidity and funding liquidity. *Review of Financial Studies*. <https://doi.org/10.1093/rfs/hhn098>
- Buldyrev, S.V., Parshani, R., Paul, G., Stanley, H.E. and Havlin, S. (2010). Catastrophic cascade of failures in interdependent networks. *Nature*. <https://doi.org/10.1038/nature08932>

- Cameron, A.C., Gelbach, J.B. and Miller, D.L. (2008). Bootstrap-based improvements for inference with clustered errors. *The Review of Economics and Statistics*, 90(3), 414-427. <https://doi.org/10.1162/rest.90.3.414>
- Carpenter, S.R., Cole, J.J., Pace, M.L., Batt, R., Brock, W.A., Cline, T. et al. (2011). Early warnings of regime shifts: A whole-ecosystem experiment. *Science*. <https://doi.org/10.1126/science.1203672>
- CFTC and SEC Staff (2010). Findings Regarding the Market Events of May 6, 2010. Report, SEC / CFTC. <https://www.sec.gov/news/studies/2010/marketevents-report.pdf>
- Chaney, A.J.B., Stewart, B.M. and Engelhardt, B.E. (2018). How algorithmic confounding in recommendation systems increases homogeneity and decreases utility. *ACM RecSys*. <https://doi.org/10.1145/3240323.3240370>
- Dakos, V., Carpenter, S.R., Brock, W.A., Ellison, A.M., Guttal, V., Ives, A.R. et al. (2012). Methods for detecting early warnings of critical transitions in time series illustrated using simulated ecological data. *PLOS ONE*. <https://doi.org/10.1371/journal.pone.0041010>
- de Moura, L. and Ullrich, S. (2021). The Lean 4 Theorem Prover and Programming Language. *CADE-28*. https://doi.org/10.1007/978-3-030-79876-5_37
- Efron, B. (1987). Better Bootstrap Confidence Intervals. *Journal of the American Statistical Association*, 82(397), 171-185. <https://doi.org/10.1080/01621459.1987.10478410>
- ESRB Advisory Scientific Committee (2019). Can ETFs Contribute to Systemic Risk? Report, ESRB. https://www.esrb.europa.eu/pub/pdf/asc/esrb.asc190617_9_canetfscontributesystemicrisk~983ea11870.en.pdf
- Fleder, D. and Hosanagar, K. (2009). Blockbuster culture's next rise or fall: The impact of recommender systems on sales diversity. *Management Science*. <https://doi.org/10.1287/mnsc.1080.0974>
- Gao, J., Barzel, B. and Barabasi, A.-L. (2016). Universal resilience patterns in complex networks. *Nature*. <https://doi.org/10.1038/nature16948>
- Hanley, J.A. and McNeil, B.J. (1982). The meaning and use of the area under a receiver operating characteristic (ROC) curve. *Radiology*. <https://doi.org/10.1148/radiology.143.1.7063747>
- Holling, C.S. (1973). Resilience and stability of ecological systems. *Annual Review of Ecology and Systematics*. <https://doi.org/10.1146/annurev.es.04.110173.000245>
- Jäger, G. and Füllsack, M. (2019). Systematically false positives in early warning signal analysis. *PLOS ONE*. <https://doi.org/10.1371/journal.pone.0211072>
- Jiang, R., Chiappa, S., Lattimore, T., Gyorgy, A. and Kohli, P. (2019). Degenerate feedback loops in recommender systems. *AIES/ACM*. <https://doi.org/10.1145/3306618.3314288>
- Mansoury, M., Abdollahpouri, H., Pechenizkiy, M., Mobasher, B. and Burke, R. (2020). Feedback loop and bias amplification in recommender systems. *CIKM*. <https://doi.org/10.1145/3340531.3412152>
- NYSE Market-Wide Circuit Breaker (MWCB) Working Group (2021). Report of the Market-Wide Circuit Breaker (MWCB) Working Group. Report, NYSE / SEC. <https://www.nyse.com/press-releases/2021/03/16/nyse-sec-market-wide-circuit-breaker-report>

[//www.nyse.com/publicdocs/nyse/markets/nyse/Report_of_the_Market-Wide_Circuit_Breaker_Working_Group.pdf](http://www.nyse.com/publicdocs/nyse/markets/nyse/Report_of_the_Market-Wide_Circuit_Breaker_Working_Group.pdf)

Page, E.S. (1954). Continuous Inspection Schemes. *Biometrika*, 41, 100-115. <https://doi.org/10.1093/biomet/41.1-2.100>

Scheffer, M., Carpenter, S., Foley, J.A., Folke, C. and Walker, B. (2001). Catastrophic shifts in ecosystems. *Nature*. <https://doi.org/10.1038/35098000>

Scheffer, M., Bascompte, J., Brock, W.A., Brovkin, V., Carpenter, S.R., Dakos, V. et al. (2009). Early-warning signals for critical transitions. *Nature*. <https://doi.org/10.1038/nature08227>

Scheffer, M., Carpenter, S.R., Lenton, T.M., Bascompte, J., Brock, W., Dakos, V. et al. (2012). Anticipating critical transitions. *Science*. <https://doi.org/10.1126/science.1225244>

Schnabel, T., Swaminathan, A., Singh, A., Chandak, N. and Joachims, T. (2016). Recommendations as Treatments: Debiasing Learning and Evaluation. ICML. <https://proceedings.mlr.press/v48/schnabel16.html>

Shumailov, I., Shumaylov, Z., Zhao, Y., Papernot, N., Anderson, R. and Gal, Y. (2024). AI models collapse when trained on recursively generated data. *Nature*. <https://doi.org/10.1038/s41586-024-07566-y>

Shumailov, I., Shumaylov, Z., Zhao, Y., Papernot, N., Anderson, R. and Gal, Y. (2025). Author Correction: AI models collapse when trained on recursively generated data. *Nature*, 640, E6. <https://doi.org/10.1038/s41586-025-08905-3>

The mathlib Community (2020). The Lean mathematical library. *CPP (ACM SIGPLAN)*. <https://doi.org/10.1145/3372885.3373824>

Walker, B., Holling, C.S., Carpenter, S.R. and Kinzig, A. (2004). Resilience, adaptability and transformability in social-ecological systems. *Ecology and Society*. <https://doi.org/10.5751/ES-00650-090205>

Whaley, R.E. (2009). Understanding the VIX. *Journal of Portfolio Management*. <https://doi.org/10.3905/jpm.2009.35.3.098>

Yeh, C.-C.M., Zhu, Y., Ulanova, L., Begum, N., Ding, Y., Dau, H.A., Silva, D.F., Mueen, A. and Keogh, E. (2016). Matrix Profile I: All Pairs Similarity Joins for Time Series: A Unifying View that Includes Motifs, Discords and Shapelets. *IEEE ICDM*, 1317-1322. <https://doi.org/10.1109/ICDM.2016.0179>

Supplementary Materials

Benchmarking Recursive-Collapse Warning Claims Under Matched False-Positive Control

David Mullett · ORCID: 0009-0004-2543-1664 · d@loopzero.org · Independent Researcher

This document contains the supplementary materials referenced in the main manuscript: one figure (S1) and four tables (S2, S3, S4, S5).

Supplementary Figure S1

Supplementary Figure S1. Fast-family segmentation and band sensitivity on the canonical markets benchmark. No fast-family comparator was accepted at 60-, 120-, or 180-minute segmentation under the prespecified equal-false-positive band [0.03, 0.07]. Under widened post-processing bands with upper cutoff 0.08, acceptance appeared only for the 60-minute AC1 configuration; the canonical 120-minute and 180-minute segmentations remained non-accepted across all tested bands.

Band	Segmentation	Band reachable	Any fast accepted	Nearest family	Nearest FP	Distance to band
[0.02, 0.08]	60 min	Yes	Yes	ac1_ews	0.0800	0.0000
[0.02, 0.08]	120 min	Yes	No	ac1_ews	0.1316	0.0516
[0.02, 0.08]	180 min	Yes	No	ac1_ews	0.1304	0.0504
[0.03, 0.07]	60 min	Yes	No	ac1_ews	0.0800	0.0100
[0.03, 0.07]	120 min	Yes	No	ac1_ews	0.1316	0.0616
[0.03, 0.07]	180 min	Yes	No	ac1_ews	0.1304	0.0604
[0.04, 0.08]	60 min	Yes	Yes	ac1_ews	0.0800	0.0000
[0.04, 0.08]	120 min	Yes	No	ac1_ews	0.1316	0.0516
[0.04, 0.08]	180 min	Yes	No	ac1_ews	0.1304	0.0504

Source: `results/frozen/comparators/markets_fast_robustness_packet_v1__20260421T175531Z/markets_fast_band_sensitivity_summary_v1.csv`.

Supplementary Table S2

Supplementary Table S2. Effect sizes with bootstrap 95% confidence intervals. Per-witness Cohen’s d, Glass’s d, and rank AUC at each benchmark/horizon (4 benchmarks \times 3 witnesses \times 3 effect measures = 36 cells), with both BCa-adjusted and percentile bootstrap confidence intervals from cluster-aware resampling (10,000 iterations). Markets uses segment-level resampling (n=38 controls + 16 events); recommender (all horizons) uses user-level resampling (n = 40,339 user clusters). Canonical h=50 group is bolded throughout. A sensitivity section flags cells where BCa and percentile CI endpoints differ by ≥ 0.05 (markets p-witness cells only — the bootstrap distribution is right-skewed at low n, and BCa is the more honest read there). Full numerics rendered deterministically by `analysis/17_render_a3_supplementary_table_s2.py` from the per-cell bootstrap output at `results/rendered/effect_sizes/a3_effect_sizes_full.csv`.

Source: `results/rendered/effect_sizes/a3_effect_sizes_full.csv` (commit d8908dd)

Generator: `analysis/17_render_a3_supplementary_table_s2.py`

Per-witness (G, p, δ) effect sizes at each benchmark/horizon with 95% BCa confidence intervals from cluster-aware bootstrap (10,000 iterations). Cohen’s d, Glass’s d, and Rank AUC are reported as complementary magnitude metrics. BCa is the primary CI method; percentile CIs are reported alongside for the cells where they differ meaningfully (sensitivity section below).

Sign convention

Predicted direction by witness (event vs control):

- **G** (amplification): event > control predicted; positive d / AUC > 0.5 confirms
- **p** (concentration): event > control predicted; positive d / AUC > 0.5 confirms
- **δ** (contraction): event < control predicted; negative d / AUC < 0.5 confirms

Bootstrap unit grain

- **Markets:** segment-level resampling (n = 38 controls + 16 events; ~30 rows per segment)
- **Recsys** (all horizons): user-level resampling (n = 40,339 user clusters; 10 rows per cluster)

Effect sizes by benchmark

Markets (Volmageddon + COVID-MWCB)

Witness	Cohen’s d [BCa 95% CI]	Glass’s d [BCa 95% CI]	Rank AUC [BCa 95% CI]
G	-0.029 [-0.169, +0.147]	-0.028 [-0.155, +0.160]	0.507 [0.459, 0.555]
p	+0.097 [-0.488, +0.941]	+0.119 [-0.412, +2.094]	0.482 [0.398, 0.614]
δ	+0.029 [-0.568, +0.617]	+0.029 [-0.563, +0.617]	0.516 [0.353, 0.680]

Recsys h=40 (off-pre-reg)

Witness	Cohen's d [BCa 95% CI]	Glass's d [BCa 95% CI]	Rank AUC [BCa 95% CI]
G	-0.214 [-0.235, -0.192]	-0.213 [-0.233, -0.192]	0.441 [0.436, 0.447]
p	+0.180 [+0.155, +0.205]	+0.172 [+0.147, +0.197]	0.555 [0.549, 0.562]
δ	-0.268 [-0.299, -0.237]	-0.219 [-0.245, -0.190]	0.415 [0.407, 0.423]

Recsys h=50 (canonical, pre-registered)

Witness	Cohen's d [BCa 95% CI]	Glass's d [BCa 95% CI]	Rank AUC [BCa 95% CI]
G	+0.100 [+0.076, +0.124]	+0.112 [+0.084, +0.139]	0.519 [0.513, 0.525]
p	+0.080 [+0.049, +0.111]	+0.073 [+0.043, +0.102]	0.531 [0.523, 0.539]
δ	-0.168 [-0.208, -0.128]	-0.125 [-0.155, -0.095]	0.457 [0.447, 0.467]

Recsys h=60 (off-pre-reg)

Witness	Cohen's d [BCa 95% CI]	Glass's d [BCa 95% CI]	Rank AUC [BCa 95% CI]
G	+0.333 [+0.310, +0.354]	+0.453 [+0.411, +0.495]	0.575 [0.570, 0.580]
p	+0.007 [-0.028, +0.043]	+0.006 [-0.026, +0.038]	0.513 [0.504, 0.522]
δ	-0.029 [-0.072, +0.016]	-0.021 [-0.053, +0.011]	0.508 [0.497, 0.520]

BCa-vs-percentile sensitivity

BCa correction matters where the bootstrap distribution is skewed (small n; right-skewed tails on small-n p-witness). Cells where $|\text{BCa endpoint} - \text{percentile endpoint}| \geq 0.05$ on either side:

Benchmark	Witness	Measure	Percentile CI	BCa CI	max Δ
Markets	p	glasss_d	[-0.492, +1.356]	[-0.412, +2.094]	0.74
Markets	p	cohens_d	[-0.589, +0.695]	[-0.488, +0.941]	0.25

Notes

- **Recsys BCa correction is empirically negligible.** Across all 27 recsys cells at $n = 40,339$, $|\text{BCa} - \text{percentile}| < 0.01$ on every endpoint. Consistent with BCa's $O(1/\sqrt{n})$ second-order correction theory: at this n the correction is below the bootstrap Monte Carlo noise floor. Percentile CIs would suffice for recsys; BCa is reported for completeness and procedural consistency with markets.

- **Markets BCa correction is substantive for the p witness.** The Glass’s d markets p cell upper bound shifts from percentile +1.357 to BCa +2.094 (54% right-shift). Bootstrap distribution is right-skewed at n=54; percentile CIs systematically understate the right tail. BCa is the honest read here.
- **Canonical h=50 is the only configuration where all three witnesses align in the predicted direction with CIs clear of 0** (bolded above). Adjacent recsys horizons degrade asymmetrically: h=40 G flips sign while p and δ hold; h=60 G strengthens while p and δ collapse to null. The pre-registered horizon delivers the cleanest signature — evidence that pre-registration was load-bearing for the bridge claim.
- **Markets row-level effects are uniformly null** (all three witnesses, all three measures, all CIs span 0 or 0.5). The directional bridge claim for markets operates at unit-level aggregation grain (mean per unit, then compare unit means across the n=38+16 segments); the row-level effect-size table above is honest data at the finer grain. See main text Cross-domain evidence section for the unit-level framing.

See also: Figure 6 (effect-size forest plot, results/figures/a3_effect_size_forest.{png,pdf}); Cross-domain evidence section of the main manuscript.

Supplementary Table S3

Supplementary Table S3. Alert-count exact-matching sensitivity check. Re-expression of the envelope-boundary matched-FP comparison (main-text Table 2) in integer alarm counts. For each panel at the canonical $k = 3$, Loopzero is reported at its envelope-boundary alarm counts (`n_control_alarmed`, `n_event_alarmed`); each comparator family’s frozen pre-registered calibration grid is searched for the operating point with the nearest `n_control_alarmed` value, with status classified as `exact_match` (comparator has an operating point at Loopzero’s exact alarm count), `bounded_gap` (Loopzero’s alarm count falls between two adjacent comparator operating points, with `gap` quantifying the calibration coverage gap), `no_overlap_above` (all comparator operating points have higher alarm counts), or `insufficient_data`. On the markets benchmark, `ac1_ews` exhibits `exact_match` at Loopzero’s envelope-boundary anchor: both methods alarm on exactly 9 of 38 controls and detect exactly 3 of 16 events. On the recommender benchmark, `variance_ews` exhibits the widest bounded gaps across Loopzero’s envelope boundary: 3559 alarms at $h = 40$ (Loopzero at 97 of 6562 controls) and 3345 alarms at $h = 60$ (Loopzero at 2 of 3996 controls), in each case with the upper-bound comparator operating point detecting all panel event units ($\text{TPR} = 1.0$). At $h = 50$, no comparator family produced a non-trivial breakpoint at Loopzero’s envelope-boundary FP of 0.002313; accordingly, $h = 50$ is reported for transparency but excluded from the cross-horizon comparator-envelope comparison. Full numerics rendered by `analysis/21_compute_a2_alert_count_exact.py` from frozen calibration data at `results/rendered/a4_roc_lowfp/a4_roc_data.parquet` and operating-point data at `results/rendered/bridge/a1_loopzero_operating_points{,_h40_h60}.csv`. Columns renamed in this rendering for compactness: `lower` and `upper` abbreviate `comp_lower` and `comp_upper`; `gap` abbreviates `gap_width_n_control`; `n_bp` abbreviates `n_breakpoints`.

Companion to `a2_threshold_path_envelope_boundary.{csv,md}`. Re-frames the envelope-boundary comparison in integer alarm counts to surface (a) discrete-FP-space coincidences as exact

alarm-count matches, and (b) linear-interpolation gaps as quantitative gap widths in alarm-count space.

Comparator alarm counts derived from $\text{round}(\text{fp_comp} * \text{panel.n_control_units})$ and $\text{round}(\text{tpr_comp} * \text{panel.n_event_units})$. Status legend:

- `loopzero_envelope_boundary` — Loopzero’s anchor at panel max FP, $k=3$
- `exact_match` — comparator has a breakpoint at exactly Loopzero’s alarm count
- `bounded_gap` — Loopzero’s alarm count falls strictly between two adjacent comparator breakpoints; `gap` records the gap size
- `no_overlap_above` — all comparator breakpoints have higher alarm counts
- `no_overlap_below` — all comparator breakpoints have lower alarm counts
- `insufficient_data` — comparator has <1 useful breakpoint

Panel: markets

Panel `n_control_units=38`, `n_event_units=16`. Loopzero at envelope boundary ($q=50$, $k=3$): **9 false alarms / 38 controls** (FP=0.236842), **3 true detections / 16 events** (TPR=0.1875).

family	status	lower (ctrl, evt)	upper (ctrl, evt)	gap	n_bp
ac1_ews	exact_match	(9, 3)	(9, 3)	0	25
cusum	no_overlap_above	—	(14, 5)	—	15
page_hinkley	no_overlap_above	—	(26, 14)	—	6
variance_ews	no_overlap_above	—	(17, 5)	—	20

Panel: recsys_h40

Panel `n_control_units=6562`, `n_event_units=33777`. Loopzero at envelope boundary ($q=50$, $k=3$): **97 false alarms / 6562 controls** (FP=0.014782), **3113 true detections / 33777 events** (TPR=0.0922).

family	status	lower (ctrl, evt)	upper (ctrl, evt)	gap	n_bp
ac1	no_overlap_above	—	(4206, 33777)	—	3
cusum	no_overlap_above	—	(4010, 33777)	—	4
matrix_profile	no_overlap_above	—	(155, 3938)	—	2
page_hinkley	no_overlap_above	—	(4206, 33777)	—	4
permutation_entropy	no_overlap_above	—	(6562, 33777)	—	1
variance_ews	bounded_gap	(0, 0)	(3559, 33777)	3559	6

Panel: recsys_h50

Panel `n_control_units=4755`, `n_event_units=35584`. Loopzero at envelope boundary ($q=50$, $k=3$): **11 false alarms / 4755 controls** (FP=0.002313), **2681 true detections / 35584 events** (TPR=0.0753).

family	status	lower (ctrl, evt)	upper (ctrl, evt)	gap	n_bp
<i>no comparator breakpoint at this boundary FP</i>	<code>insufficient_data</code>	—	—	—	0

Panel: recsys_h60

Panel n_control_units=3996, n_event_units=36343. Loopzero at envelope boundary (q=50, k=3): **2 false alarms / 3996 controls** (FP=0.000501), **2004 true detections / 36343 events** (TPR=0.0551).

family	status	lower (ctrl, evt)	upper (ctrl, evt)	gap	n_bp
<code>acl</code>	<code>no_overlap_above</code>	—	(3464, 36343)	—	3
<code>cusum</code>	<code>no_overlap_above</code>	—	(3430, 36343)	—	4
<code>matrix_profile</code>	<code>no_overlap_above</code>	—	(35, 3938)	—	2
<code>page_hinkley</code>	<code>no_overlap_above</code>	—	(3464, 36343)	—	4
<code>permutation_entropy</code>	<code>no_overlap_above</code>	—	(3996, 36343)	—	1
<code>variance_ews</code>	<code>bounded_gap</code>	(0, 0)	(3345, 36343)	3345	6

Supplementary Table S4

Supplementary Table S4. Cluster-robust sensitivity at scenario grain (markets benchmark). Per-witness effect sizes (Cohen’s d, Glass’s d, rank AUC) on the markets benchmark at the A3 segment grain (n = 54 segments) and the B3 scenario grain (n = 7 clusters: 2 event scenarios — `volmageddon_2018_xiv` with 8 segments and `covid_mwcb_2020_03_18` with 8 segments; 5 control scenarios — `covid_noncollapse_2020_03_11` with 8 segments, `volmageddon_control_2018_01_29` with 8 segments, `volmageddon_control_2018_02_08` with 8 segments, `covid_noncollapse_2020_03_13` with 7 segments, `volmageddon_control_2018_01_25` with 7 segments). Bootstrap iterations: 10,000 per cell; CI level: 0.95; RNG seed for scenario grain: 43 (distinct from A3 segment grain seed: 42). For p|Glass’s d at scenario grain, 2 of 10,000 iterations produced degenerate samples (control SD ≈ 0 from same-scenario cluster resamples); finite-filter applied to remaining 9,998 iterations. All other 8 cells: n_degenerate = 0. Scenario-grain CIs are reported as sensitivity, not primary inference; the segment-grain baseline (Supplementary Table S2) remains the primary report.

Cluster composition

Event-side scenario clusters (derived from `unit_id` parsing; n=2):

Cluster	Segments
<code>volmageddon_2018_xiv</code>	8

Cluster	Segments
covid_mwcb_2020_03_18	8

Control-side scenario clusters (n=5):

Cluster	Segments
covid_noncollapse_2020_03_11	8
volmageddon_control_2018_01_29	8
volmageddon_control_2018_02_08	8
covid_noncollapse_2020_03_13	7
volmageddon_control_2018_01_25	7

Total cluster units: 7 (2 event + 5 control), down from 54 segment units in A3.

Methodological framing

Cluster-aware bootstrap (10,000 iterations) at scenario grain. Reported as a **dependence-sensitivity diagnostic** at $n = 2$ event clusters; at this sample size the bootstrap intervals are not reliable conservative inferential intervals. Wild cluster bootstrap (Cameron, Gelbach & Miller 2008) — the methodologically appropriate response to the small-cluster regime — is deferred to follow-up work.

Effect sizes at scenario grain (B3)

Witness	Measure	Point	Percentile 95% CI	BCa 95% CI
G	cohens_d	-0.0293	[-0.0916, +0.0489]	[-0.0932, +0.0473]
G	glasss_d	-0.0285	[-0.0934, +0.0472]	[-0.0938, +0.0472]
G	rank_auc	+0.5073	[+0.4569, +0.5581]	[+0.4520, +0.5530]
p	cohens_d	+0.0966	[-0.3309, +0.4082]	[-0.3285, +0.4313]
p	glasss_d	+0.1188	[-0.2952, +0.7102]	[-0.2950, +0.7102]
p	rank_auc	+0.4823	[+0.4376, +0.5310]	[+0.4361, +0.5305]
delta	cohens_d	+0.0286	[-0.1534, +0.1993]	[-0.1534, +0.1993]
delta	glasss_d	+0.0287	[-0.1610, +0.1928]	[-0.1610, +0.1928]
delta	rank_auc	+0.5162	[+0.4495, +0.5773]	[+0.4495, +0.5757]

Side-by-side: A3 segment grain vs B3 scenario grain (BCa 95% CI)

Witness	Measure	A3 segment grain (n=54)	B3 scenario grain (n=7)	CI width ratio
G	cohens_d	[-0.1686, +0.1469]	[-0.0932, +0.0473]	0.45×
G	glasss_d	[-0.1552, +0.1598]	[-0.0938, +0.0472]	0.45×
G	rank_auc	[+0.4592, +0.5552]	[+0.4520, +0.5530]	1.05×
p	cohens_d	[-0.4884, +0.9409]	[-0.3285, +0.4313]	0.53×

Witness	Measure	A3 segment grain (n=54)	B3 scenario grain (n=7)	CI width ratio
p	glasss_d	[-0.4123, +2.0944]	[-0.2950, +0.7102]	0.40×
p	rank_auc	[+0.3979, +0.6141]	[+0.4361, +0.5305]	0.44×
delta	cohens_d	[-0.5682, +0.6167]	[-0.1534, +0.1993]	0.30×
delta	glasss_d	[-0.5632, +0.6174]	[-0.1610, +0.1928]	0.30×
delta	rank_auc	[+0.3527, +0.6799]	[+0.4495, +0.5757]	0.39×

Supplementary Table S5. Reproducibility anchor hashes

Freeze-manifest SHA-256 hashes for the empirical components anchoring all results in this paper. Each frozen directory additionally contains a LOCK_NOTE.md documenting that freeze’s scientific and editorial scope.

Component	Freeze path	SHA-256
Recsys benchmark freeze state (canonical)	results/frozen/movielens 25m_recursive_frontier_public_v1__benchmark_freeze_state.json	050aa725e6608f659b3f7eb1 03731bb7fbabaa23aeefdc4b 11043999b7fed4cf
Recsys contract freeze	results/frozen/movielens 25m_recursive_frontier_public_v1__contract_freeze.json	f361d937cc07cbb946753ac9 e5e2d1d386c8706a6bb43841 229ec846fd69ecd6
Recsys manuscript freeze state	results/frozen/movielens 25m_recursive_frontier_public_v1__manuscript_freeze_state.json	bc8542cc0b76cdfad9726a40 85c760d38ed7ace24772f0e3 c6103fba962891b8
Markets comparator merged state (v2)	results/frozen/comparators/markets_comparator_merged_state_v2__20260421T174702Z/freeze_manifest.json	784895418953b1646bd40eb7 b5266e39901326b1335b2ec5 f2390b70af4642c7
Markets fast robustness packet (v1)	results/frozen/comparators/markets_fast_robustness_packet_v1__20260421T175531Z/freeze_manifest.json	f8f8c5c58d10796d4b715452 82a8b352c47dc9590fc268fc b96cfb84c181adec
Witness-direction bridge state (v3, canonical)	results/frozen/bridge/witness_direction_bridge_state_v3__20260422T130759Z/freeze_manifest.json	bd47e75851fcaea1e6d843f9 b74156ec036ddb487ca76e81 5d7b6fb0cf258f94
Manuscript two-domain state (v1)	results/frozen/manuscript/two_domain_paper_state_v1__20260422T134303Z/freeze_manifest.json	1763b04cb128a274dd12313a 8cccdb2a04e2845d176d3444 d6214e0aafe2e1d5

Component	Freeze path	SHA-256
Recsys horizon sensitivity manifest (covers h=40, h=50, h=60)	results/manifests/movielens25m_recursive_frontend_public_v1_horizon_sensitivity_summary.json	b5d7ef3b5ca10f9e446a9792bc7d677a323913c66c087e753c6de944a8b7f215
MovieLens-25M source archive (upstream)	https://files.grouplens.org/datasets/movielens/m1-25m.zip (GroupLens; not redistributed)	8b21cfb7eb1706b4ec0aac894368d90acf26ebdfb6aced3ebd4ad5bd1eb9c6aa

Engine: movielens_recursive_replay_engine v1.0.0 (item_item_collaborative_filtering, hash 56c1cff225d60c09). Recsys contract: SHA-256 2e256b255a7f074c1516d70315ebb216241a4a7e8aba2db88b194417705fd71d. All hashes are SHA-256 in lowercase hexadecimal.

Generated 2026-05-28 alongside the main manuscript v17.17 render. Companion to the main paper PDF.